Atlantic Multidecadal Variability (AMV) in the Norwegian Earth System model

Master thesis in Climate Dynamics

Julie Solsvik Vågane

June 2020

supervised by
Noel Keenlyside and Ingo Bethke

University of Bergen
Faculty of Mathematics and Natural Sciences
Geophysical Institute

Abstract

The causes of low-frequency sea surface temperature (SST) variations in the Atlantic, known as Atlantic Multidecadal Variability (AMV), are debated. AMV has climatic impacts on for instance hurricane activity and Sahel rainfall, and understanding AMV can improve decadal predictions. While some discuss whether AMV arises due to external forcing, the ocean dynamics or the thermodynamic atmosphere-ocean interaction, others question the very existence of AMV. In this thesis, I look at the Norwegian Earth System Model (NorESM), investigating low-frequency variability and possible drivers for AMV in the North Atlantic. I compute a heat budget and a multiple linear regression (MLR) model, and investigate the influence of the dynamics and thermodynamics on AMV on different time scales and regions. I use the North Atlantic Oscillation (NAO) and the Atlantic Meridional Overturning circulation (AMOC) to characterize the large-scale impacts associated with ocean and atmospheric circulation patterns. The MLR model with NAO and AMOC, manages to explain 20.5 % of the temperature tendency on an interannual time scale, and 34.8 % on a decadal time scale in the subpolar gyre (SPG). In the tropics, the variance explained is smaller, only explaining 6.5 % interannually and 9.6 % decadally. Through a comparison with observations, I found that the AMOC amplitude is underestimated and the SST is off by over 1°C. This may influence the performance of the MLR model. Finally, I present some ideas for improving the MLR model and the possibility for decadal predictions.

Acknowledgements

A huge thank you to my supervisors, Ingo and Noel, who guided me through this thesis, even in times of Corona. Thank you for paying attention to details, for basically teaching me how to program, and for keeping me on track.

Thank you to my friends and family, for listening to my frustrations and joys, and for distracting me from constantly thinking about SST variations. A big thank you to my roomies, who survived my enthusiastic presentations of programming breakthroughs, and for keeping me going with food and Pepsi Max. Thank you to my friends at GFI, for five beautiful years, filled with loud conversations, hard work and long breaks.

And thank you to Salt, for reminding me that there are more important things in life than my master thesis.

Acronyms

AMOC	Atlantic Meridional Overturning Circulation
AMV	Atlantic Multidecadal Variability
DIV	heat divergence
HFLX	surface heat flux
MLR	multiple linear regression
NAO	North Atlantic Oscillation
NorCPM	Norwegian Climate Prediction Model
NorESM	Norwegian Earth System Model
SPG	subpolar gyre
SST	sea surface temperature
std	standard deviation
TEND	temperature tendency

Contents

1. Introduction

The Atlantic Multidecadal Variability (AMV) is a decadal to interdecadal variation in sea surface temperature (SST) in the North Atlantic Ocean [Keenlyside and Ba, 2010], with colder and warmer periods. The phenomenon has been known since Jacob Bjerknes wrote an article about it in 1964 [Bjerknes, 1964]. Since then, there has been research on the different mechanisms driving the AMV, as well as the possibility to predict it. Still, the concept is not fully understood, and there is an ongoing debate about the driving forces of AMV.

One motivation for researching AMV is climate change attribution, to better understand the underlying mechanisms of our changing climate. Attribution is essential for the evaluation and development of climate models and prediction systems, that aim to produce reliable climate future projections and predictions, especially on a regional scale. The combined effect of the AMV-related natural climate variability and global warming could amplify the temperature anomaly in naturally warm periods, and smoothen out the anomalies when AMV is in a colder period. Another reason for studying AMV, is its climate impact. The AMV pattern has been associated with for instance Sahel rainfall [Zhang and Delworth, 2006], European summer climate [Sutton and Hodson, 2005], summer Arctic sea ice extent [Zhang, 2015] and Atlantic hurricane activity [Goldenberg et al., 2001]. By more accurate predictions of AMV, we may better predict climate change, and prepare for the extreme weather associated with AMV.

There is a discussion about the factors driving and influencing AMV. Keenlyside and Ba [2010] present two categories of causes; internal climate variability and external forcing. Internal climate variability refers to processes within the Earth's systems, such as El Niño and the ocean circulation, while external forcing is driven by components outside the system, e.g. solar and volcanic forcing and anthropogenic greenhouse gas and aerosol emissions. There are several internal and external processes that may influence AMV, for instance the Atlantic Meridional Overturning Circulation (AMOC) [e.g. Zhang et al., 2019], the North Atlantic Oscillation (NAO) [e.g. Clement et al., 2015] and volcanic [Otterå et al., 2010] and anthropogenic [Booth et al., 2012] aerosols. It is challenging to separate the effect of ocean dynamics and thermodynamics, however, due to interactions between the ocean and the atmosphere, and as instrumental climate records are relatively short. This problem can be overcome by the use of paleoproxy records (which unfortunately are highly uncertain) and climate model output.

This thesis aims at understanding aspects of AMV as simulated in the Norwegian Earth system model (NorESM). The focus is on the internal variability, and the variations in the North Atlantic SST. My working hypothesis is that both the dynamic and thermodynamic processes have a signif-

icant impact on AMV, and that the model has some low-frequency variability that reflects AMV. I look at the dynamic and thermodynamic aspects of AMV, by studying ocean heat divergence and the surface heat flux, as well as AMOC and NAO. My main research question is "What are the driving forces for AMV?". Further, this research question is subdivided into smaller questions, that will be discussed through the Results and Discussion chapters:

- Is there an enhanced low-frequency variability in the North Atlantic SST in the NorESM simulations? If yes, is there a dominant period?
- How is the annual column-averaged temperature tendency in the North Atlantic related to the ocean dynamics and thermodynamic atmosphere-ocean interaction? And how are these relations changing on different time scales and in different regions?
- How is the surface heat flux related to the North Atlantic Oscillation (NAO), and the ocean heat transport divergence to the Atlantic Meridional Overturning Circulation (AMOC)? How much of the variance in temperature tendency can be explained by NAO and AMOC?
- How well does the model simulate the observations of sea surface temperature (SST), surface heat flux (HFLX), North Atlantic Oscillation (NAO) and Atlantic Meridional Overturning Circulation (AMOC)?

To address these questions, I use output from an ensemble of historical simulations from NorESM. I estimate the internal variability as a deviation from the ensemble mean, that is the full SST signal minus the estimated external forcing. I look at different time scales and regions, and compute a heat budget and a multiple linear regression model to estimate the contribution from the ocean dynamics and the thermodynamic ocean-atmosphere interaction to the temperature variations. I perform this analysis for both the whole North Atlantic, and for smaller regions: the subpolar gyre (SPG) and a tropical region. To assess the realism of the model simulations, I compare the results with observations, where these are available.

My main findings are that there is an enhanced low-frequency variability in the North Atlantic, that both the ocean heat transport divergence and the surface heat flux play an important part in SST variations, and while NAO is most important on interannual time scales, AMOC is more important on a decadal time scale.

2. Theory and background

2.1 What is AMV?

The Atlantic Multidecadal Variability (AMV) is low-frequency sea surface temperature (SST) variations in the North Atlantic. A time series of the observed SST anomalies in the North Atlantic (0-60°N, 7.5-75°W) is shown in Fig. 2.1. It shows relatively warm (cold) periods shaded in red (blue). There are warmer periods around 1860-1880, 1940 and after the 2000s, and colder periods around 1905-1925 and 1970-1975. These low-frequency SST variations can for instance counteract SST increases due to global warming [Zhang et al., 2007].

AMV is also referred to as the Atlantic Multidecadal Oscillation (AMO), because earlier studies assumed there was a preferred time scale of 70-80 years [Gulev et al., 2013, Keenlyside et al., 2015, Yeager and Robson, 2017]. Today, many studies based on climate models show a broader spectrum of low-frequency signals, instead of one spectral peak. AMV is varying on different time scales and in different regions [Zanchettin et al., 2014], and is influenced by different components. I have chosen to focus this thesis on the interannual to interdecadal SST variations in the subpolar gyre (SPG) and a tropical region in the low-latitude North Atlantic.

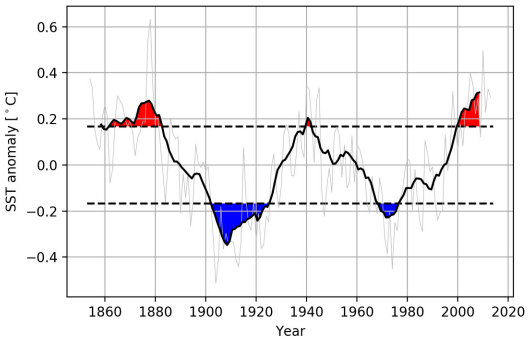

Figure 2.1: Annual observed SST anomalies (deviation from mean) in the North Atlantic, from 1854 to 2014. The dotted horizontal lines show the standard deviation (std), and the red and blue areas are periods of SST larger than one std. The grey line shows the annual SST anomalies, and the black line shows the 10 years low-pass filtered SST anomalies. The observations are from the National Oceanic and Atmospheric Administration (NOAA) [Huang et al., 2017].

The spatial pattern of AMV is shown in Fig. 2.2. Especially in the subpolar gyre region, the difference between the warmer and colder period is considerable. There is a maximum in the Labrador Sea, with 0.4°C average difference between the cold and the warm periods.

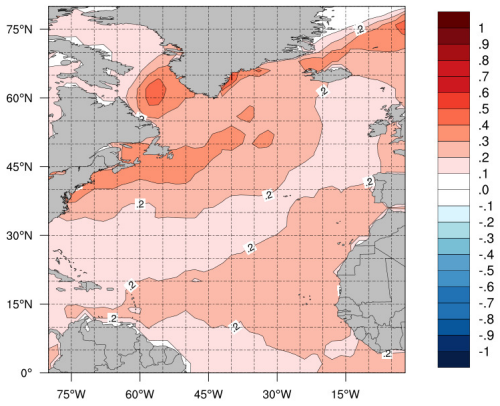

Figure 2.2: The spatial pattern of the observed AMV. It is computed as the difference between the periods of SST higher and lower than one standard deviation of the observed AMV index (Fig. 2.1). The observations are from NOAA [Huang et al., 2017].

2.2 Regions of AMV in the North Atlantic

In this thesis, I have defined the subpolar gyre (SPG) as the box from 48°N to 65°N, 65°W to 10°W. There are several other definitions, as in e.g. Lohmann et al. [2008] (50-65°N, 60-15°W), Robson et al. [2012] (50-66°N, 60-10°W) and Robson et al. [2018] (50-65°N, 60-10°W), but they largely cover the same area. The definition used in this thesis is motivated by the spatial AMV pattern (Fig. 2.2), and the climatological barotropic stream function presented in Fig. 2.3. In particular, I define the SPG by the box in the North of Fig. 2.3 that covers most of the the region where the barotropic mass stream function is cyclonic in the North Atlantic. This region also covers most of the region with the largest difference between the warmer and colder periods (Fig. 2.2). The same definition of the SPG is used in papers as Lohmann et al. [2009], and later adopted by Counillon et al. [2016].

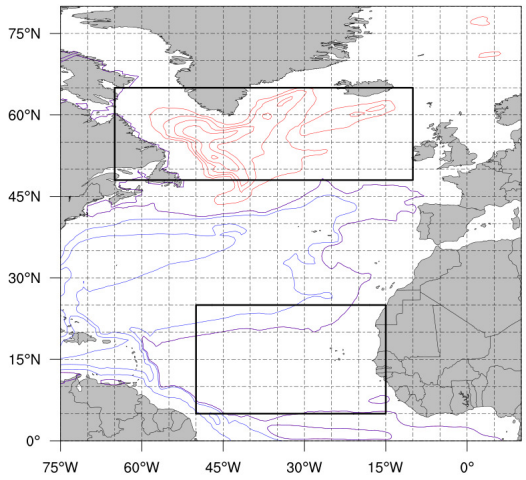

Figure 2.3: The barotropic climatological streamfunction, averaged over 1850-2014. Red is anticyclonic (negative streamfunction), and blue is cyclonic (positive stream function). The two boxes defined in the North Atlantic are marked with black boxes.

The dynamics in the SPG are largely influenced by the Atlantic Meridional Overturning Circulation (AMOC) [Delworth et al., 1993]. AMOC is the zonal mean large scale ocean circulation in the North Atlantic. The strong, northward ocean current, the Gulf Stream, transports heat into the SPG, and when the water cools around the Greenland, Iceland and Norwegian Seas, it sinks and returns towards lower latitudes [Keenlyside et al., 2015]. Due to the cold surface temperatures, there is a relatively deep mixed layer in the SPG.

Further, I defined a tropical region, 5°N to 25°N, 50°W to 15°W, the southernmost box in Fig. 2.3. This region has higher SST, smaller influence from the Gulf Stream, smaller seasonal variations, and a shallower mixed layer than the SPG. The climatological barotropic stream function

(Fig. 2.3) shows little long-term circulation in this region. However, this region is of interest due to for instance the hurricane activity, that also shows a multidecadal variability [Yan et al., 2017]. Comparing the SPG region and the tropical region will give an impression of how AMV is varying spatially in the North Atlantic.

2.3 The heat budget and AMV

The vertically integrated temperature tendency can be calculated through equation, Eq. 2.1. The vertically integrated temperature tendency (TEND) depends on the vertically averaged heat divergence (DIV) and the surface heat flux (HFLX).

$$\int_{h_{bot}}^{0} (\frac{dT}{dt})dh = -\int_{h_{bot}}^{0} (\nabla \cdot T\vec{u})dh + \frac{HFLX}{\rho c_p}, \qquad \vec{u} = u, v, w \tag{2.1}$$

where $\int_{h_{bot}}^{0} (\frac{dT}{dt})dh$ is the vertically integrated temperature tendency (TEND), $\int_{h_{bot}}^{0} (\nabla \cdot T\vec{u})dh$ is the vertically averaged temperature divergence (DIV), and $\frac{HFLX}{\rho c_p H}$ is the surface heat flux (HFLX) over density (ρ), heat capacity (c_p) and depth of the layer (H). The density is considered a constant, $\rho_0 = 1028$ kg/m^3, as the changes in density are relatively small. The temperature divergence can be called a dynamic component, driven by the ocean. This term includes both the advection and the horizontal mixing due to unresolved eddies that are parametrized in the model. The HFLX, the thermodynamic component, is mostly driven by the atmosphere, although it can depend on the ocean on longer time scales [Gulev et al., 2013]. The HFLX consists of both the radiative (longwave and shortwave) and the turbulent (sensible and latent) fluxes. The largest effect of HFLX is seen in the mixed layer, the upper part of the ocean. Hence, to get a change in SST, there has to be a vertical heat flux at the surface, and/or a heat flux divergence.

The thermodynamic and dynamic components have different influences on AMV in different regions, and on different time scales. Yeager et al. [2012] discuss how the thermodynamics and ocean dynamics impact the heat budget in the SPG in the 1990's shift from colder to warmer temperatures. They concluded that both the temperature advection and the surface heat flux played large roles, but that the surface heat flux had the largest impact on a short time scale (the abruptness), while the ocean advection was dominating on a decadal time scale. However, other studies indicate that the shift was independent of the sudden shift in NAO, and rather a result of the previous positive NAO [Lohmann et al., 2009, Robson et al., 2012].

There is an ongoing discussion about the components driving AMV; if it is mainly ocean heat transport divergence, thermodynamic ocean-atmosphere interaction or external forcing, as well as a discussion about the very existence of AMV. Many studies use Atlantic Meridional Overturning Circulation (AMOC) and North Atlantic Oscillation (NAO) as physical quantities to describe the influence of the thermodynamics and dynamics on AMV. AMOC is closely related to poleward ocean heat transport [Zhang et al., 2019]. The NAO is the dominant pattern of large-scale winter time variability in the North Atlantic region, and it is closely related to turbulent heat fluxes. Cau-

tions must be made when assigning the surface heat flux as NAO and the heat divergence to AMOC, as atmospheric and oceanic variability also influence heat flux and ocean heat transport. However, these two are recognized as the dominant signals. Through the next sections, I will present studies supporting all of these points of view.

2.4 The influence of the atmosphere on AMV

NAO can be defined as the normalized difference in pressure between the Azores high and the Icelandic low [Visbeck et al., 2001, Hurrell et al., 2003]. However, NAO impacts climate in other ways than merely pressure differences. During positive NAO phases, there are more storms travelling over the North Atlantic [Hurrell et al., 2003], and an atmospheric circulation that favors cold air advection from the Arctic over the SPG region. This acts to cool the SPG thermodynamically, as well more dynamic wind-stress related effects, like Ekman pumping [Visbeck et al., 2003]. This strong cooling can drive winter time deep convection. For example, NAO variations have been linked to changes in Labrador sea water formation, that have in turn been linked to variations in AMOC [Yeager and Robson, 2017].

As a null-hypothesis for stochastic climate, the Hasselmann [1976] model is a common approach. Hasselmann calculated the change in the SST as a result of atmospheric noise and changes in a one-layer ocean without dynamics, a slab ocean. More recent studies build on this model, using a slab ocean model to explain AMV [e.g. Cane et al., 2017, Clement et al., 2015]. Clement et al. [2015] reproduced the multidecadal variation pattern in SST with a stochastic atmosphere forcing and slab ocean only. They suggested that stochastic, atmospheric forcing is the only driver for AMV, and that the ocean is merely responding to the atmosphere. This is a debated study however, and will be further discussed in section 2.5.

Cane et al. [2017] presented a study implying that AMV can be a product of low pass filtering. The study emphasizes the role of the external forcing, and is also regarding the ocean's impact as white noise, based on the slab ocean model. They used a noise-forced model, and applied a low-pass filter, filtering out the higher frequencies. The filter is argued to create non-existing correlations, and to be sensitive to the cutoff frequency. In addition, the study stresses the importance of the difference between correlation and causality; that a correlation does not automatically imply causality. Cane et al. [2017] conclude that white noise, mainly from the atmosphere, is the primary driver of AMV.

Most studies state that both NAO and AMOC have an important impact on AMV [e.g. Marshall et al., 2001, Yeager and Robson, 2017, Robson et al., 2012, Garuba et al., 2018]. Additionally, there can be possible impacts from NAO on AMOC, and feedbacks from the ocean back to NAO [Marshall et al., 2001, Yeager and Robson, 2017]. NAO can impact Ekman layers, ocean gyres, and thermohaline circulation [Marshall et al., 2001]. For instance, a positive NAO strenghtens the Gulf Stream, bringing more saline water into the SPG and increases the mixed layer depth. A deeper mixed layer is harder to cool from the atmosphere, and gives a relative heating [Yamamoto et al., 2020]. These mechanisms make the separation of the dynamic and thermodynamic influence more complicated.

The relation between the NAO and SST resembles a tripole pattern on seasonal timescales [Visbeck et al., 2001, 2003, Marshall et al., 2001]. Positive NAO is correlated with colder SST in the SPG (negative correlation), a northward shift of the Gulf Stream, and stronger heat flux in the SPG (positive correlation) [Visbeck et al., 2003]. As well as a colder SPG, positive NAO is correlated with a stronger SPG [Lohmann et al., 2008]. 10 years after the positive NAO, the SPG gets warmer and weaker. This is not a direct delayed response of the NAO, but a response to enhanced AMOC and a spinup of the SPG [Eden and Jung, 2001, Lohmann et al., 2008]. The AMOC response is however related to the preceding positive NAO, once again demonstrating the relation between the dynamics and thermodynamics. Also worth mentioning in this context, is the difference between correlation and causality; even though two variables are correlated (correlation), a change in one variable is not necessarily causing a change in the other variable (causality).

2.5 The influence of the ocean on AMV

The Atlantic Meridional Overturning Circulation (AMOC) is often used as an estimate of the ocean influence on AMV. AMOC is the circulation in the North Atlantic that includes poleward heat transport in the top of the water column, sinking in the North Sea, an equatorward transport at intermediate depths, and rising in the area where the Gulf Stream starts. Unfortunately, there are few observations of AMOC, but it has been reconstructed through so-called AMOC fingerprints, which are other observed variables that correlate with AMOC [Zhang et al., 2019]. These fingerprints show correlations to AMV and key elements of AMV, indicating that AMOC could be an important driver of AMV. This is supported by correlations between AMOC and AMV in climate models [Zhang et al., 2019]. Model studies also show a significant contribution from AMOC on SST variability [Schmith et al., 2014].

Several studies [Wang et al., 2014, Zhang et al., 2019, Yan et al., 2018] show that the magnitude of AMOC variability is underestimated in many climate models. One of the challenges, is that the modelled AMOC is too shallow, leading to a too weak meridional heat transport [Zhang et al., 2019]. As a consequence, the impact of AMOC on AMV may be underestimated. The lack of long-term observations of AMOC is also a challenge in estimating the influence of AMOC on AMV. Reconstructions of past climate suggest a link between AMV and AMOC strength [Knight et al., 2005].

As mentioned in section 2.4, there is a discussion about the slab ocean model. In a comment to Clement et al. [2015], Zhang et al. [2016] stated that the main driver of AMV is ocean heat transport convergence, emphasizing the multidecadal time scale of AMV. A review study by Zhang et al. [2019] also points out that the slab ocean model fails to represent several parts of AMV, for instance the observed multidecadal variability. The impact of NAO and AMOC on AMV is depending on the time scale, with NAO having a larger impact on shorter time scales, and AMOC on longer time scales [Marshall et al., 2001, Keenlyside et al., 2015, Garuba et al., 2018]. Hence, the atmosphere generally has a more instantaneous impact on SST than the ocean dynamics. A case study of the ocean warming in the 1990s, showed that the SST increase was a delayed effect of positive NAO and a strengthened AMOC [Robson et al., 2012, Lohmann et al., 2009].

In addition to the individual impact of AMOC and NAO on AMV, there are interaction mechanisms between the ocean and the atmosphere [e.g. Timmermann et al., 1998, Gulev et al., 2013, Peings and Magnusdottir, 2014]. There is evidence of a coupled air-sea mode, with an influence of the atmosphere on the ocean, as well as a feedback from the ocean to the atmosphere [Timmermann et al., 1998]. One of these mechanisms is the influence of the ocean on the multidecadal surface heat flux. Filtered (11 years running mean) SST observations and surface turbulent heat flux reconstructions show a correlation of up to 0.77 in the North Atlantic [Gulev et al., 2013], indicating that the ocean is driving the atmosphere on multidecadal time scales [see also Peings and Magnusdottir, 2014].

2.6 External forcing driving AMV

Several studies claim that external forcing, not NAO or AMOC, is the main driver of AMV [Watanabe and Tatebe, 2019, Booth et al., 2012, Mann et al., 2014, 2020]. These studies look at external forcing from e.g. volcanoes [Otterå et al., 2010], aerosol-cloud microphysics [Booth et al., 2012] and sulphate aerosols [Watanabe and Tatebe, 2019]. Otterå et al. [2010] discuss internal and external interaction (e.g. volcanic eruptions favoring positive NAO affecting AMOC), rather than a distinct separation.

The direct role of the external forcing has a larger effect in the low-latitude North Atlantic than in the SPG, where the internal variability seems to be more important [Watanabe and Tatebe, 2019]. One specific period that has raised attention, is the North Atlantic cooling around 1950-1970. Several studies [Otterå et al., 2010, Booth et al., 2012, Mann et al., 2020] suggest this part of the variability to be a result of aerosol forcing.

Mann et al. [2014, 2020] discuss the methods in separating the internal variability from the full signal. A common method is to consider the internal SST variability as the linearly detrended SST. Mann et al. [2014, 2020] are questioning this method, and suggest that it results in an overestimated amplitude of the SST variability, and a bias in the phase of the AMV. Another approach is to estimate the external forcing as a multimodel ensemble mean, which results in a less distinct multidecadal variation. However, this assumes that the model perfectly reproduces the externally forced signal, which is not necessarily the case.

2.7 AMV and decadal prediction

As AMV is a low-frequency variability, it could possibly be predicted on longer time scales. A better understanding of AMV, as well as the impact from AMOC and NAO, might increase the decadal prediction skill. The research on decadal predictions is a fast changing field, and through the past 15 years there has been large progress. Newer research on decadal climate predictions show that the skill of decadal predictions increases with the inclusion of more members and initialisation from observations [Yeager et al., 2018, Kushnir et al., 2019, Smith et al., 2019]. For instance, a run with more members will increase the signal-to-noise ratio, so that the signal is more discernible, which

is especially important as current models tend to underestimate the signal-to-noise ratio [Smith et al., 2019]. However, decadal predictions still have some challenges to overcome to make accurate predictions.

Decadal prediction skill can be assessed by comparing hindcast model runs with observations. However, few observations of variables like surface heat fluxes, subsurface temperatures and meridional overturning circulation [Keenlyside et al., 2008] can make this assessment difficult. Also, the existing observational data sets are often rather short, compared to the period of multidecadal variations. The lack of observations is also problematic in the initialization of the models [Keenlyside et al., 2008]. Other challenges are the high computational costs of decadal predictions [Yeager et al., 2018], and incomplete understandings of the underlying physics behind processes such as AMV [Kushnir et al., 2019]. The costs of decadal predictions are high, due to for instance annual initializations, runs with several members and the length of each prediction [Yeager et al., 2018].

Yan et al. [2018] showed that a greater AMOC variability (closer to the observed values) gives a higher predictability in the Atlantic Ocean, and that use of the slab ocean model gives a lower decadal prediction skill. Similar studies also emphasize the importance of AMOC in decadal predictability [Latif et al., 2004, Robson et al., 2018]. The region of the highest decadal predictability in the North Atlantic is the SPG [Keenlyside et al., 2008, Yeager et al., 2012, Robson et al., 2018], suggesting a larger impact of AMOC on AMV in this region.

2.8 AMV in some climate models

A study on comparison of AMV performance showed large individual differences between coupled general circulation models [Ba et al., 2014]. For instance, the models had differing AMV periods, and only 5 of 10 models showed a clear relation between AMOC and AMV. In CMIP5 models, there are indications of multidecadal variation in both AMV and AMOC, but with differing amplitudes and frequencies [Zhang and Wang, 2013]. In difference to the study by Ba et al. [2014], Zhang and Wang [2013] found that most CMIP5 models showed a relation and interaction between AMV and AMOC. The Norwegian Earth System Model (NorESM) showed a periodicity of 20 years for both SST variability and AMOC [Bentsen et al., 2013]. Hence, there are large variations in the findings in the different studies and models. Due to lack of reliable, long-term observational records, it is difficult to judge which models are more correct, and if they show a higher skill due to correct understanding of the underlying dynamics or not. However, studying the impact of NAO and AMOC in one model, which both have been identified to play roles in AMV, provides insight into the decadal predictability of this specific model. This can lead to improved understanding and predictions of the AMV.

3. Methods

3.1 Hierarchy of models

3.1.1 The Norwegian Earth System Model

The data in this thesis is based on an ensemble run of the CMIP6 version of the Norwegian Climate Prediction Model (NorCPM1) [Bethke, in prep.]. The run is done by the Bjerknes Climate Prediction Unit team. The atmospheric model has a latitude-longitude resolution of 1.9 x 2.5° for atmosphere and land, with 26 hybrid sigma-pressure levels. The ocean has a nominal resolution of 1 x 1°, with the pole rotated over Greenland, and increasing resolution towards both the equator and the poles [Bethke, in prep]. In the ocean there are 51 isopycnic levels, and a mixed layer varying in time and space. NorCPM1 is based on the Norwegian Earth System Model version 1 (NorESM1-ME) [Bentsen et al., 2013], combined with the ensemble Kalman filter for data assimilation. The ensemble Kalman filter is assimilating the observations directly into a coupled climate system [Counillon et al., 2016, Wang et al., 2017]. Data assimilation is applied for the entire model state of the ocean component, and the assimilation is currently using SST and temperature-salinity profile observations. NorCPM1 also contributed to CMIP6 with assimilation experiments and initialised retrospective predictions, which could be looked at in a possible follow up of this study. Focusing on the historical experiment, has the advantages of closed heat budgets and a clean separation of internal from externally forced variability. In this thesis, I will not use the runs with the data assimilation.

All model analysis in the thesis is based on the CMIP6 historical experiment of NorCPM1, that covers the period 1850 to 2014, using observed external forcing. This experiment does not include any data assimilation, and I will refer to the model as NorESM in the thesis. The model run has 30 ensemble members, with slightly different initial conditions. The variation within one member shows the result of both internal and external variability, while the mean of all members (ensemble mean) gives an estimate of the externally forced variation. Hence, the variation in one member minus the ensemble mean is an estimate of the internal variability. These internal SST variations are the objective of this thesis. The large ensemble of members in this analysis allows for a more robust estimate of the external and internal variability, and increases the signal-to-noise ratio. Based on the output from NorCPM1, a heat budget and a multiple linear regression (MLR) model are constructed to investigate the mechanisms governing simulated AMV in NorCPM.

3.1.2 The heat budget

I computed the heat budget for the 30 simulations based on Eq. 2.1, with temperature tendency, temperature divergence and surface heat flux. The heat budget provides results for looking at the correlations and influences of heat flux and temperature divergence on temperature tendency, and to quantify the variability over time. Also, the heat budget is a verification of NorESM, by checking that the heat budget is closed.

Technically, temperature tendency and temperature divergence are not completely accurate terms, as the components are multiplied with density, specific heat capacity and layer thickness. The terms get the unit W/m^2, like fluxes. However, as these are the regular heat budget terms, the names remain the same, even though the units are different. The surface heat flux (HFLX) is an output of the NorESM run. The monthly temperature tendency is calculated at each level as in Eq. 3.1:

$$\frac{dT^*}{dt} = (tempinslvl_{month} - tempinslvl_{month-1}) \cdot c_p \cdot \rho \cdot d \cdot \frac{1}{t} \tag{3.1}$$

where tempinslvl is a measure of the instantaneous temperature at end of averaging period [°C], c_p is the specific heat capacity [J/(kg°C)], ρ is the density [kg/m^3], d is the thickness of the layer [m] (accounting for the influence of pressure on layer depth), and t is the time given in seconds per month. I have denoted the temperature as T*, to distinguish it from temperature, as the temperature tendency integrated over one layer has a unit of $J/(sm^2) = W/m^2$. The monthly temperature divergence is calculated at each level as in Eq. 3.2:

$$\nabla \cdot T\vec{u} = -\frac{(uhflxlvl[i+1,j] - uhflxlvl[i,j]) + (vhflxlvl[i,j+1] - vhflxlvl[i,j])}{area[i,j]} \tag{3.2}$$

where uhflxlvl[i,j] and vhflxlvl[i,j] are the heat fluxes in Watts in x- and y-direction at the point [i,j], for one specific level with a certain thickness, and area[i,j] is the area of the grid cell [i,j] in m^2. The temperature divergence (integrated over one layer) also has the unit of W/m^2.

Further, I compute annual averages of the heat budget components, as I focus on interannual to decadal variability. The temperature tendency and the temperature divergence are then vertically integrated over all layers, while the surface heat flux only is calculated at the top of the ocean. Fig. 3.1 shows the vertically integrated heat budget for the North Atlantic, hence the residual from the three terms in Eq. 2.1, for one month (February 1850, member 1). The month and member is chosen for illustrative purposes, but is representative for the whole period and all members.

An interesting feature is that the heat budget has the largest deviation north of 60°N. In this area, there is an alternation between positive and negative deviations, maybe due to a numerical error. This error is largely decreased for spatial averages, and the residual is much smaller than the variations in the individual components in the heat budget. The sum of the heat budget indicates

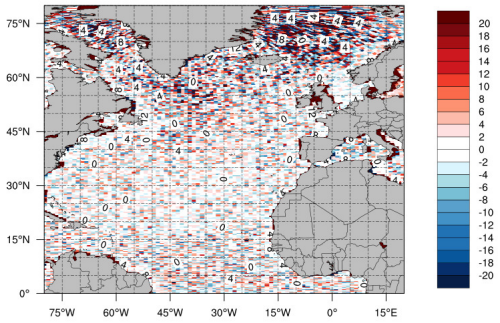

Figure 3.1: The vertically averaged heat budget over the North Atlantic, for February 1850, member 1.

a virtually closed budget. The cause of this residual is still unclear, but a look on the box average supports the alternating errors cancelling.

In order to look at the variability over time, I looked at the box averaged variables in the North Atlantic. The boxes are defined as in Fig. 2.3, with the SPG and a tropical region. Each cell in the given box is given a weight, depending on longitude and latitude, so that the largest grid cells have a larger impact on the average. The weighting is done as shown in Eq. 3.3:

$$weights = area \cdot mask \tag{3.3}$$

where area is the area of each grid cell, depending on latitude and longitude, and mask is giving weight only to the grid cells within the given latitudes and longitudes (0 weight is given to grid cells outside the given range). The weights are then normalized, so that the sum of all weights add to 1.

By this box averaging, I can plot time series that represent the two regions in the North Atlantic. Fig. 3.2 shows the box averaged heat budget for 1850 to 2014 in the SPG, for the first member of the ensemble run. Also this figure indicates a closed heat budget, with a mean residual of 0.001 W/m^2 in the SPG, and very small interannual variations. Hence, the heat budget is considered closed on a regional scale, but with some local errors.

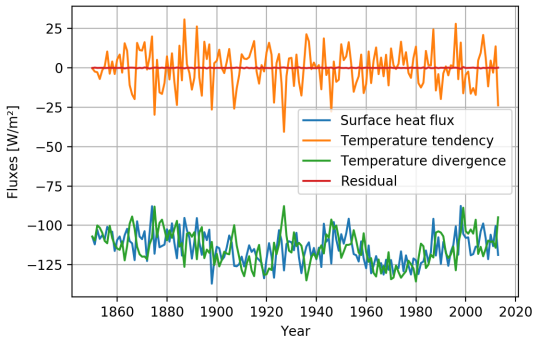

Figure 3.2: The box averaged heat budget in the SPG for 1850 to 2014, member 1.

3.1.3 The multiple linear regression model

A multiple linear regression analysis is performed in order to estimate the combined influence and relative importance of several independent variables (predictors) on one dependent variable (predictand). With two predictors, the outcome, y_{reg}, is determined through Eq. 3.4:

$$y_{reg} = c_1 \cdot x_1 + c_2 \cdot x_2, \tag{3.4}$$

where y_{reg} is the predictand, c_1 and c_2 are the regression coefficients, and x_1 and x_2 are the predictors.

If the two predictors are dependent, the regression coefficients must be calculated so that the overlapping part is not accounted for twice. The least square method is applied to compute a y_{reg} that minimizes the squared error. The least square method is minimizing the squared error between y_{reg} and y, as shown in Eq. 3.5:

$$\frac{\partial \Sigma (y - y_{reg})^2}{\partial c_{1,2}} = \frac{\partial \Sigma (y - c_1 \cdot x_1 - c_2 \cdot x_2)^2}{\partial c_{1,2}} = 0 \tag{3.5}$$

The minimization is then done by taking the derivative of Eq. 3.5 by the chain rule, with respect to c_1 and c_2. This results in a set of equations, shown in Eq. 3.6. By setting the partial derivative to zero, the difference between y and y_{reg} is minimized.

$$\Sigma 2 \cdot (y - c_1 \cdot x_1 - c_2 \cdot x_2) \cdot \frac{\partial (y - c_1 \cdot x_1 - c_2 \cdot x_2)}{\partial c_1} = 0 \tag{3.6a}$$

$$\Sigma 2 \cdot (y - c_1 \cdot x_1 - c_2 \cdot x_2) \cdot \frac{\partial (y - c_1 \cdot x_1 - c_2 \cdot x_2)}{\partial c_2} = 0 \tag{3.6b}$$

Solving the set of equations for c_1 and c_2 with linear algebra, the two regression coefficients can finally be calculated as in Eq. 3.7 and 3.8:

$$c_1 = \frac{\Sigma x_1 y \Sigma x_2^2 - \Sigma x_2 y \Sigma x_1 x_2}{\Sigma x_1^2 \Sigma x_2^2 - (\Sigma x_1 x_2)^2} = \frac{cov(x_1, y) \cdot var(x_2) - cov(x_2, y) \cdot cov(x_1, x_2)}{var(x_1) \cdot var(x_2) - cov(x_1 x_2)^2} \tag{3.7}$$

$$c_2 = \frac{\Sigma x_2 y \Sigma x_1^2 - \Sigma x_1 y \Sigma x_1 x_2}{\Sigma x_1^2 \Sigma x_2^2 - (\Sigma x_1 x_2)^2} = \frac{cov(x_2, y) \cdot var(x_1) - cov(x_1, y) \cdot cov(x_1, x_2)}{var(x_1) \cdot var(x_2) - cov(x_1 x_2)^2} \tag{3.8}$$

Hence, the estimate of the predictand, y_{reg}, is given by the two time series x_1 and x_2, weighted by the two coefficients, c_1 and c_2. The coefficients depend on the variance of the predictors (var(x_1) and var(x_2)), and the covariance between the predictors and the predictand (cov(x_1,y), cov(x_2,y) and cov(x_1,x_2)). The covariance and variance are estimated through Eq. 3.13. This calculation of the regression coefficients works both if the predictors are dependent or independent. If the two predictors are independent, the expression can be simplified, as the covariance then will be zero.

In this thesis, MLR is performed in order to estimate the combined influence and relative importance of HFLX, x_1, and DIV, x_2, on temperature tendency, y, as well as NAO, x_1, and AMOC, x_2, on the temperature tendency, y. To prepare the time series, I subtracted the mean to get the anomalies. The normalizing of the time series is taken into account in the MLR coefficients. AMOC is defined as the overturning stream function (mmflxd) at the depth of maximum flow at 26.5°N. The unit is Sverdrup [Sv], and AMOC is calculated as in Eq. 3.9:

$$AMOC = (mmflxd(26^\circ N) + mmflxd(27^\circ N)) \cdot 0.5 \tag{3.9}$$

Fig. 3.3 indicates that there is a relatively high correlation between the AMOC stream function with depth, and the meridional heat transport at 48°N. This is an indication that AMOC at 26.5°N could give a good estimate of the heat transport to the SPG. Another reason for choosing 26.5°N is the position of the RAPID array at 26°N, an observational array of AMOC strength [Smeed et al., 2019].

The NAO index is defined as the normalized winter-mean (December through March) pressure difference between Reykjavik and Lisbon, without units. I compare the winter NAO with annual

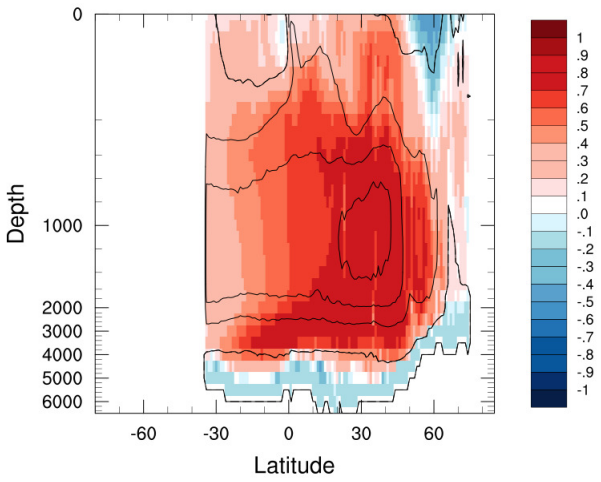

Figure 3.3: Annual correlation with depth, between the AMOC stream function and the meridional heat transport. The correlation is computed for every member, and then averaged. The black lines show the climatological stream function with depth.

TEND, e.g. NAO of winter 1850/1851 with TEND in 1851. It is calculated as in Eq. 3.10:

$$NAO = \frac{SLP_{Lisbon} - \overline{SLP_{Lisbon}}}{std(SLP_{Lisbon})} - \frac{SLP_{Reykjavik} - \overline{SLP_{Reykjavik}}}{std(SLP_{Reykjavik})} \tag{3.10}$$

where SLP_{Lisbon} and $\text{SLP}_{Reykjavik}$ is the sea level pressure at Lisbon and Reykjavik, respectively, and std(SLP) is the standard deviation of the sea level pressure.

To quantify the variance explained by the components (HFLX and DIV or AMOC and NAO) individually, I compared the variance explained by the MLR model (varexpl_{MLR}), to the variance explained by each component (varexpl_{x_1} and varexpl_{x_2}). The variance explained can be estimated from equation 3.11:

$$varexpl_{MLR} = (1 - \frac{var(y - y_{reg})}{var(y)}) \cdot 100\% \tag{3.11}$$

Similarly, varexpl_{x_1} and varexpl_{x_2} can be estimated from Eq. 3.12. As already discussed, correlation between the two predictors can lead to an overlap. In this case, correlating predictors will give $\text{varexpl}_{MLR} \neq \text{varexpl}_{x_1} + \text{varexpl}_{x_2}$.

$$varexpl_{x_1} = (1 - \frac{var(y - c_1 \cdot x_1)}{var(y)}) \cdot 100\% \tag{3.12a}$$

$$varexpl_{x_2} = (1 - \frac{var(y - c_2 \cdot x_2)}{var(y)}) \cdot 100\% \tag{3.12b}$$

Another, probably more common approach for investigating relative contribution, would be to run a simple regression on each component individually. I decided to look at relative importance by setting c_1 and c_2 respectively to zero, to look at the isolated contribution from x_1 and x_2. The two approaches are slightly different, as the method chosen here will exclude the common contribution from the components. Both approaches provide information about the relative contributions, but the interpretations are slightly different.

3.2 Observations

The observations used for verifying the model are from the National Oceanic and Atmospheric Administration (NOAA) [Huang et al., 2017], the WHOI OAFlux project [Yu et al., 2011], The National Center for Atmospheric Research (NCAR) [Hurrell et al., 2020] and the British Oceanographic Data Center [Smeed et al., 2019]. An overview of the observational data is given in Table 3.1. The observations are available for different periods and with different temporal resolution.

Table 3.1: Overview of observational data.

	Available at	**Period**	**Time step**
SST	*https* : *//psl.noaa.gov/data/gridded/ data.noaa.ersst.v5.html* (sst.mnmean.nc)	1854-2019	monthly
HFLX	*ftp* : *//ftp.whoi.edu/pub/science/oaflux/ data_v3/monthly/netheat_*1983 − 2009*/*	1984-2009	monthly
NAO	*https* : *//climatedataguide.ucar.edu/climate* − *data/hurrell* − *north* − *atlantic* − *oscillation* − *nao* − *index* − *station* − *based*	1864-2014	annual
AMOC	*https* : *//www.rapid.ac.uk/rapidmoc/ rapid_data/datadl.php*	2004-2019	daily

A difference map of the modelled SST minus the observed SST is shown in Fig. 3.4. The model is overestimating the SST in the red areas (modelled SST is higher than observed SST), and underestimating the SST in the blue areas (modelled SST is lower than observed SST). The model seems to have a cold bias in the Nordic Seas, and in the subtropics. There is a warm bias in the Labrador Sea, and in the central subpolar North Atlantic.

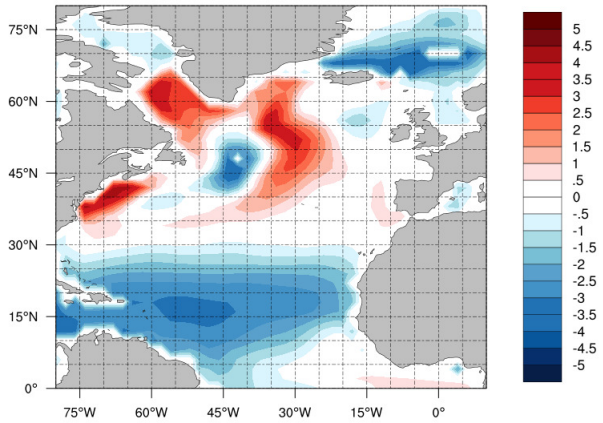

Figure 3.4: Difference map between averaged SST [°C] (1854-2014) from observations and the first member of the NorCPM run. The red (blue) areas indicate a warmer (colder) model than the observations.

The HFLX difference map is shown in Fig. 3.5. In the subtropics, there is close to no difference between the model and the observations. In the SPG, on the contrary, there are differences of up to 100 W/m^2, both underestimating and overestimating the observed HFLX. The model might have a biased position of the Gulf stream. This could explain why the model is overestimating the HFLX in the west of the SPG, and overestimating the HFLX in the eastern part.

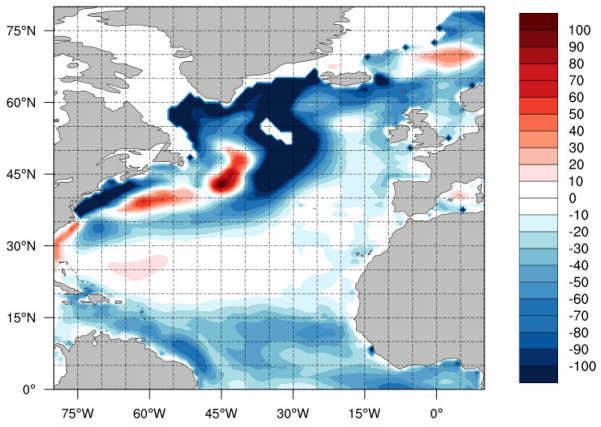

Figure 3.5: Difference map between HFLX [W/m^2] from observations and model. The red (blue) areas indicate a stronger (weaker) HFLX in the model than the observations.

3.3 Data processing

To process the data from NorESM, I used Python and Jupyter Notebook (www.python.org and www.jupyter.org). The following subsections describe the calculations and computations of correlations, filters, power spectrum and maps.

3.3.1 Correlations

Temporal and spatial correlations, autocorrelations and cross correlations provide information about how variables are varying and covarying. The correlation coefficient is a measure of the strength of a relation between two variables. It can be estimated through Eq. 3.13:

$$\begin{aligned} r(x,y) &= \frac{cov(x,y)}{std(x)std(y)}, \\ std(x)^2 = var(x) &= \frac{1}{N} \cdot (\Sigma(x-\bar{x}))^2, \\ cov(x,y) &= \frac{1}{N}\Sigma(x-\bar{x})(y-\bar{y}) \end{aligned} \tag{3.13}$$

where r(x,y) is the correlation coefficient, cov(x,y) is the covariance, std(x) is the standard deviation, and var(x) is the variance (which equals std squared). For smaller samples, N-1 could give a more accurate result, but as this data set has a larger sample size (N>30), the total sample number, N is used. The standard deviation (std(x) and std(y)) is a measure of the variations in the sample, and the covariance (cov(x,y)) is an estimate of the shared portion of the variance of x and y. In short, the correlation coefficient is the covariance over the standard deviation for x and y.

The autocorrelation is the correlation of a time series with the time shifted versions of itself, for positive and negative time lags. The autocorrelation is a measure of the memory in a time series. It is given as the autovariance (covariance of one variable) over the variance, and can be estimated through Eq. 3.14:

$$\rho(x,x)(\tau) = \frac{cov(x,x)(\tau)}{var(x)} \tag{3.14}$$

where ρ (x,x) τ is the autocovariance, τ is the lag time, cov(x,x)(τ) is the autocovariance, and var(x) is the variance.

Similarly, the cross correlation is an estimate of the relation between a time series of one variable, to another variable's lagged time series. As the autocorrelation, it is given as the covariance over the standard deviation for both variables:

$$\rho(x,y)(\tau) = \frac{cov(x,y)(\tau)}{std(x)std(y)} \tag{3.15}$$

The cross correlation can indicate if one variable is leading the other, with a lagged influence instead of an immediate correlation. However, it is important to notice the difference between correlation (a relation between two variables) and causality (influence of one variable on another variable). Correlation does not necessarily imply causality.

3.3.2 Filters and time averaging

The raw output data from the model has a monthly time step. To exclude the seasonal signal in the data, I used annual averaged data, with each month weighted by its length.

For further averaging, the running mean filter is used, through the convolution function in python, numpy.convolve. By filtering out the high-frequency variability, the long term, low-frequency variability is detected. The convolution is done as shown in Eq. 3.16.

$$(a * v)[n] = \sum_{m=-\infty}^{\infty} a[m]v[n-m] \tag{3.16}$$

where a and v are time series, with respective sizes n and m. The asterix (*) symbolizes the convolution. Sometimes, v is called a convolution kernel, giving weights to the time series a. In this case, v is simply a series of 1/N, assigning the same weight to every position in the window. N sets the size of the convolution window; a lower value increases the number of points, decreasing the smoothing of the time series. The convolution filter works as a running mean filter, and is often referred to as a "low-pass filter", due to the emphasis on lower frequencies.

3.3.3 Power spectrum

A power spectrum shows the power for different frequencies (or periods) of a time series. In this thesis, I use the power spectrum to investigate the periods of the SST variability. To distinguish the power spectrum from red noise, I compared it with the red noise spectrum. The red noise spectrum, or red spectrum, represents the null-hypothesis by Hasselmann [1976], presented in section 2.4. A consistent deviation from the red spectrum could indicate variabilities different from the null-hypothesis. To compute the power spectrum, the red spectrum and the 90th percentile of the red spectrum, I used an edited version of the function "periods" from pystuff.py (available at https://github.com/davidmnielsen/pystuff). The power spectrum is calculated using a periodogram, calculating the spectral density of the SST time series. Similarly, the red spectrum is the periodogram of red noise, produced by the SST time series.

For the average power spectrum, all members are included in the estimate of the periodogram. The red-noise uncertainty range for the averaged spectrum over 30 members is considerable smaller than the uncertainty of the spectrum calculated from a single member. The edited version of pystuff.py is adapted to produce a red noise spectrum for the ensemble-averaged power spectrum, having an additional optional parameter that specifies the number of members used in the computation of the averaged spectrum.

3.3.4 Maps

To look at the spatial pattern of the variables, as well as spatial difference and correlations, I made maps of the North Atlantic. These are computed with PyNGL (https://www.pyngl.ucar.edu). The resolution of the maps depends on the variables computed. The resolution is higher for the NorESM1 variables, than for the observations. All maps are first averaged over the relevant period. Further, when for instance looking at spatial correlations between two variables, I averaged the correlation at each grid cell over all ensemble members. The ensemble-averaging is done after the correlation calculation, as I want to look at the average correlation over all members, not the correlation of the ensemble mean.

3.3.5 Uncertainties

As already mentioned, a 30 member ensemble has an increased signal-to-noise ratio, compared to a single member model run. The uncertainty in the runs gives an estimate of the variance between

the ensemble members. One way to estimate the uncertainty, is the 25th and 75th percentile, also known as the first and third percentile. Half of the ensemble members will fall within this range. For the red spectrum in the low-frequency analysis, I used the 90th percentile, to give a more precise estimate of the member variance. Still, 10 % of the members will fall outside the 90th percentile. The percentiles are computed with the numpy function "percentile" in python.

4. Results

4.1 Time series

The first results from the analysis of NorESM, are the time series of sea surface temperature (SST) (Fig. 4.1a and 4.2a) and surface heat flux (HFLX) (Fig. 4.1b and 4.2b). These are annual mean values, with each month weighted by its length. All 30 ensemble members are included in colors, showing the variation in the members. The black dotted line is the ensemble mean, which is an estimate of the externally forced variability.

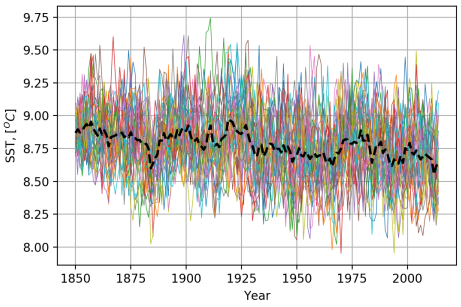

(a) Annual SST in the SPG

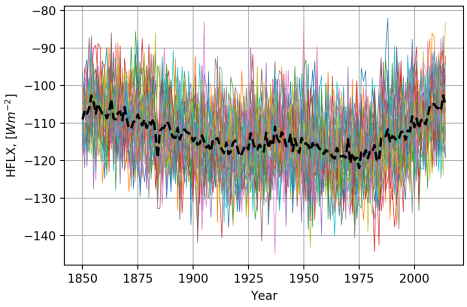

(b) Annual HFLX in the SPG

Figure 4.1: Annual mean of SST and HFLX in the SPG, with all members (in colors) and ensemble mean (dashed, black), from 1850-2014.

In the SPG (Fig. 4.1), there is a cooling trend in the SST of around half a degree from 1850 to 2014. The SST varies from 8 to 9.75°C. HFLX has negative values in this region, indicating that the ocean is losing heat to the atmosphere. The loss of heat in the ocean is decreasing after 1975. In the tropical region (Fig. 4.2), the most prominent pattern from the ensemble mean is the SST heating from around 1980, most likely related to global warming. In both the SPG and the tropics, there are some smaller "dips" in the SST. These arise due to natural variations, as for instance volcanic eruptions, and to incomplete filtering of the internal variability. The focus of this thesis will be on the internal variability, that is the variability in each member with respect to the externally forced signal (i.e., the ensemble mean).

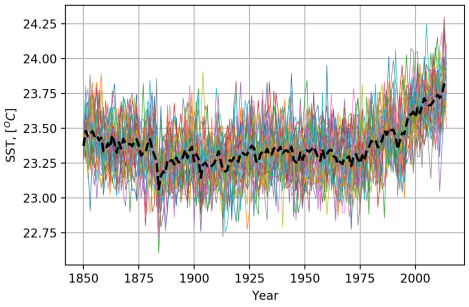

(a) Annual SST in the tropical region

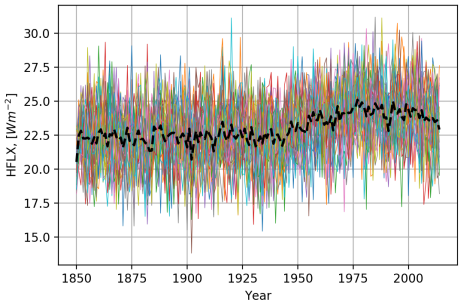

(b) Annual HFLX in the tropical region

Figure 4.2: Annual mean of SST and HFLX in the tropical region, with all members (in colors) and ensemble mean (dashed, black), from 1850-2014.

4.2 Low frequency variability

A single member's deviation from the ensemble mean gives an estimate of the the internal SST variability in that member.. Fig. 4.3 shows the SST anomaly (SST minus time evolving ensemble mean), for the first member only, box averaged over the SPG (Fig. 4.3a) and the tropical region (Fig. 4.3b). The red areas represent periods of SST larger than the average standard deviation (averaged over all ensemble members), while the blue ones represent periods which are lower than the average standard deviation (std). From this member, there seems to be some long term variability in both regions. However, there is a lower std in the tropical region, indicating smaller amplitudes in the tropical region SST variations compared to the SPG.

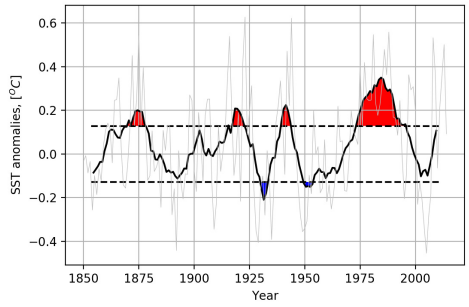

(a) SST anomalies, SPG

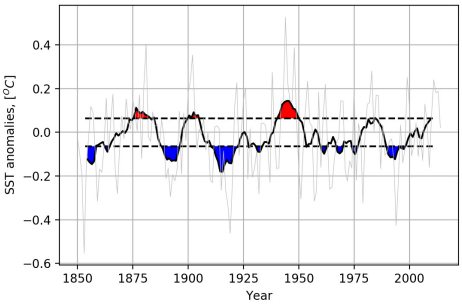

(b) SST anomalies, tropical region

Figure 4.3: Annual SST anomalies in the SPG (left) and the tropical region (right), for the first member of the ensemble run. The anomalies are found by subtracting the ensemble mean. The horizontal, dotted lines show the average std (averaged over all ensemble members, annual values), and the red and blue areas are periods of SST larger than one std. The grey lines show the annual SST anomalies, and the black lines show the 10 years low-pass filtered SST anomalies.

To further investigate the periodicity of this internal variability, Fig. 4.4 to 4.6 show the power spectrum for SST in the SPG. The individual SST spectra, for member 3 (Fig. 4.4a) and 15 (Fig. 4.4b), indicate that there is some low-frequency variability, with periods of 55 and 33 years, respectively. All of the members show low-frequency variability above the 90th percentile, but with different peaks. Fig. 4.5, shows the average of all the spectra in the SPG. The average SST spectrum shows a broader spectrum of powers higher than the 90th percentile of the average red spectrum, with periods of 20-60 years. The observed SST spectrum in the SPG is also included, in Fig. 4.6, with indications of a low-frequency variability with a period of 80 years.

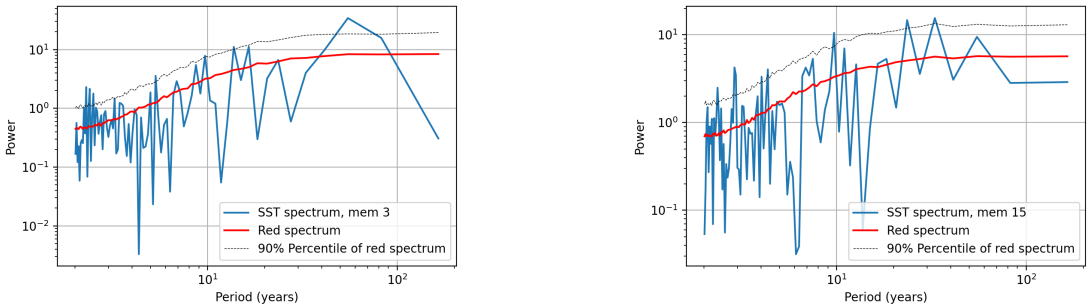

(a) Power spectrum, member 3

(b) Power spectrum, member 15

Figure 4.4: Power spectrum for member 3 (left) and 15 (right) (blue) in the SPG, red spectrum for the respective members (red), and 90th percentile of the red spectrum (dotted). These members are selected for illustrative purposes.

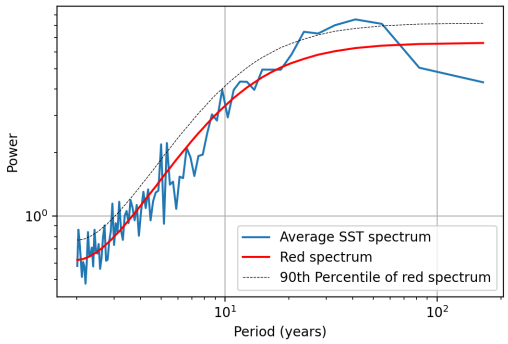

Figure 4.5: Average power spectrum for SST anomalies (average of spectrum for all members) (blue) in the SPG, average red spectrum (red) and 90th percentile of average red spectrum (dotted).

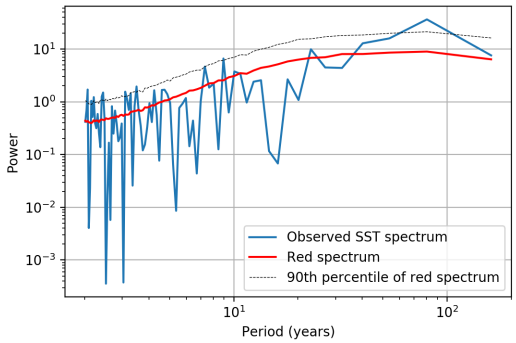

Figure 4.6: Power spectrum for observed SST anomalies (blue) in the SPG, observed red spectrum (red) and 90th percentile of red spectrum (dotted).

The power spectrum in the tropical region is showing a similar behaviour, see Fig. 4.7a and Fig. 4.7b. All individual power spectra have at least one frequency with power above the 90th percentile of the red spectrum, but for higher frequencies than in the SPG. The power of the SST variations is in general weaker in the tropical region than in the SPG, especially on longer time scales (periods over 10 years). For the average spectrum, Fig. 4.8, there is little indication of a persistent low-frequency variability. The tropical region has a lower maximum power than in the SPG, and the average period for maximum power is 9 years, compared to 41 years in the SPG. The observed SST spectrum in the tropical region (Fig. 4.9) shows little indications of a low-frequency variability, although there is some increased power around periods of 50 years. As presented in the Theory section, one would expect about 10 % of the spectra to be outside the 90th percentile. The observed power spectrum shows enhanced power for the lower frequencies than the modelled SST.

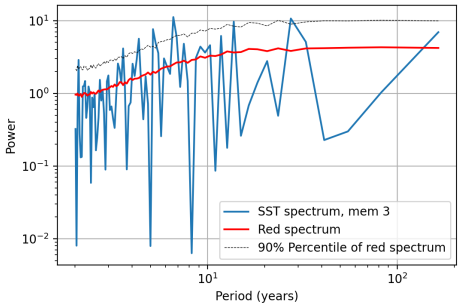

(a) Power spectrum, member 3

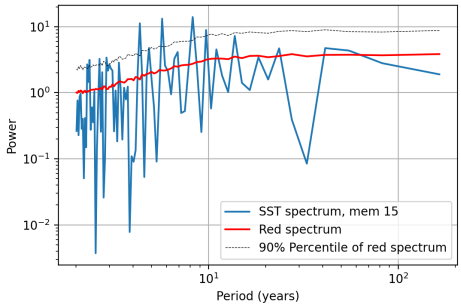

(b) Power spectrum, member 15

Figure 4.7: Power spectrum for member 3 (left) and 15 (right) (blue) in the tropical region, red spectrum for the respective members (red), and 90th percentile of red spectrum (dotted).

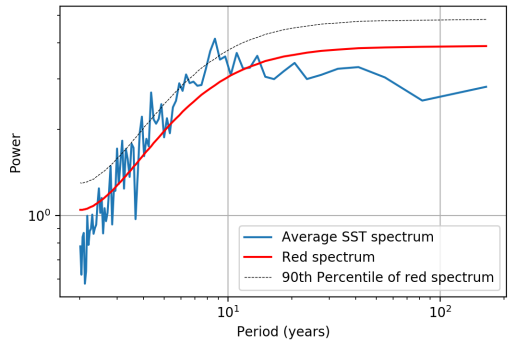

Figure 4.8: Average power spectrum for SST anomalies (average of spectrum for all members) (blue) in the tropical region, average red spectrum (red) and 90th percentile of average red spectrum (dotted).

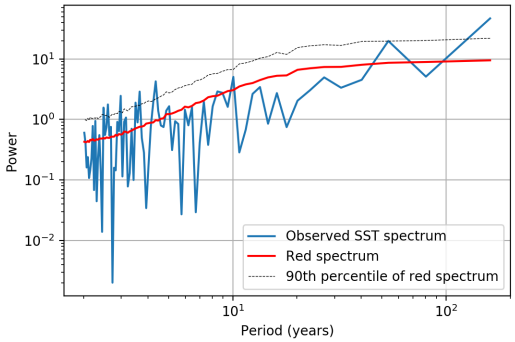

Figure 4.9: Power spectrum for observed SST anomalies (blue) in the tropical region, observed red spectrum (red) and 90th percentile of red spectrum (dotted).

The spatial pattern of the modelled AMV is presented in Fig. 4.10, computed as the difference between the warmer and colder SST periods. The model shows a strong difference between colder and warmer periods in the central SPG region, with a maximum of 0.7 °C. In difference to the observed spatial AMV pattern (Fig. 2.2), there are smaller differences in the tropics and subtropics.

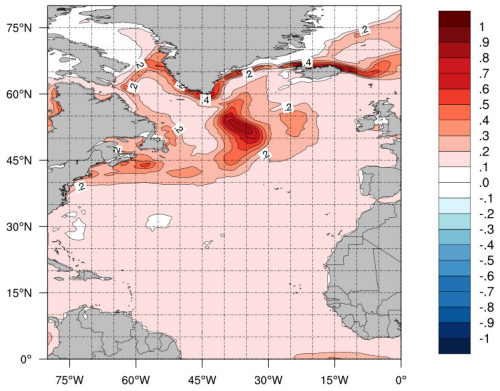

Figure 4.10: The spatial pattern of the modelled AMV, member 1. It is computed as the difference between the periods of SST higher and lower than one standard deviation of the AMV index (Fig. 4.3).

4.3 Correlation analysis

Autocorrelations provide information about the memory in a time series. Figure 4.11a shows the autocorrelation for the annual mean SST anomaly in the SPG, for the first member in the ensemble run. There is a strong autocorrelation between the years, indicating that there is a "memory" in the ocean. The autocorrelation for the annual mean HFLX is shown in Figure 4.11b. In contrast to the SST autocorrelation, there is little correlation between the years in HFLX, indicating little "memory" in the atmosphere. Additionally, there are regional differences in the North Atlantic, with for instance a less persistent ocean memory in the tropics (not shown). The strength of the autocorrelation could be an indication of the predictability, which will be further discussed in the Discussion.

The spatial correlations provides information about the spatial pattern of the relation between two variables. Fig. 4.12 shows that NAO variability is related to a tripole pattern in winter (DJFM) SST, corresponding well with the theory 2.4 [Visbeck et al., 2001, 2003, Marshall et al., 2001]. Positive NAO (large pressure difference between Lisbon (high pressure) and Reykjavik (low pressure)), is correlated with lower than usual temperatures in the SPG and the tropics, and higher than usual temperatures in the mid-North Atlantic region. Stronger winds and cold air advection from the Arctic is cooling the SPG under these conditions [Visbeck et al., 2003].

Correlation analysis show that SST tendency and vertically averaged temperature tendency (TEND) are well related in the SPG. In both the heat budget and the multiple linear regression model, I used TEND as an estimate for the SST variation. Using TEND instead of SST simplifies the heat budget, but the approximation is not perfect. Fig. 4.13 shows the SST tendency and

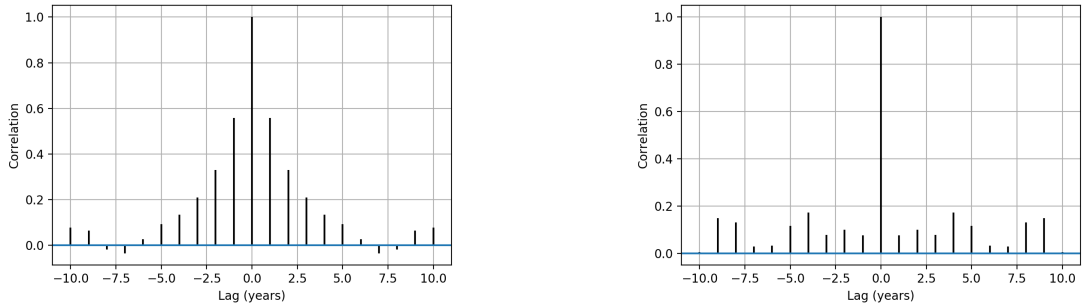

(a) Autocorrelation for SST

(b) Autocorrelation for HFLX

Figure 4.11: Autocorrelation of annual time series, for the first member of the ensemble run, for SST and HFLX. The autocorrelation is mirrored around lag = 0.

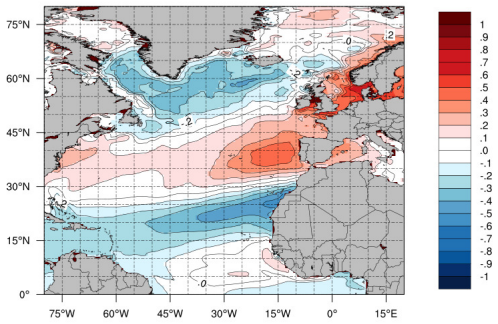

Figure 4.12: Averaged correlation map for 1850-2014, between NAO and winter SST (Dec-Mar). The correlation maps are computed for each member, and then the correlation maps are averaged.

TEND correlation for annual values (4.13a) and 10 years low-pass filtered data (4.13b). Especially in the SPG, TEND is a good approximation for SST tendency, with correlation coefficients up to 0.9 on longer time scales. In the tropical region, the correlations have a maximum of 0.5, and the approximation is thus not very good here. However, this work is more focused on the SPG region.

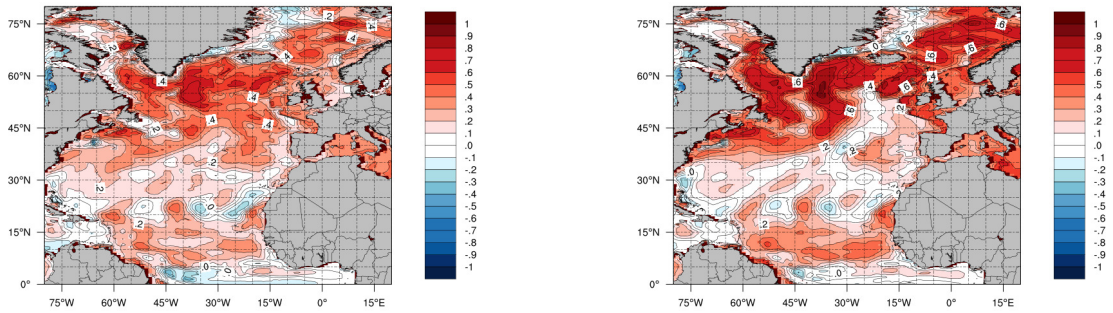

(a) SST tendency and TEND, unfiltered

(b) SST tendency and TEND, filtered

Figure 4.13: Correlation map for full period (1850-2014), SST tendency (surface) and temperature tendency (full column). The correlation maps are computed for each member, and then the correlation maps are averaged. The filter is a 10 years low-pass filter.

4.4 The heat budget

The heat budget is calculated from three components: temperature tendency (TEND), heat divergence (DIV) and surface heat flux (HFLX). While TEND and DIV is calculated at each depth, HFLX is only given at the surface (as the name implies). The complete heat budget is given in Eq. 4.1, where TEND ($\frac{dT}{dt}$) and DIV ($\nabla \cdot T\vec{u}$) is vertically integrated. Eq. 4.1 is a rewriting of Eq. 2.1, including a fourth term, R, which represents the residual of the heat budget. The residual term is small when looking at the full heat budget, but will be central when looking at the heat budget in the mixed layer (section 4.4.5).

$$\int_{h_{bot}}^{0} (\frac{dT}{dt} \cdot \rho c_p) dh + \int_{h_{bot}}^{0} (\nabla \cdot (T\vec{u}) \cdot \rho c_p) dh - HFLX = R, \qquad \vec{u} = u, v, w \tag{4.1}$$

where h_{bot} is the bottom of the ocean, $\rho = 1028$ kg/m^3 is the density (considered constant), and $c_p = 3990$ J/(kgK) is the specific heat capacity.

The subsequent subsections will present the total heat budget, followed by a presentation of the different components of the heat budget, with time series and spatial correlations. From now on, TEND and DIV will refer to the vertically integrated TEND and DIV multiplied with ρ and c_p, and all terms in the heat budget are given in W/m^2.

4.4.1 Total heat budget

Fig. 4.14 shows the four terms in the heat budget, with TEND (orange), DIV (green), HFLX (blue) and residual (red), all from the first member of the ensemble run. The SPG (Fig. 4.14a) and the tropical region (Fig. 4.14b) have opposite signs for the HFLX and the DIV terms. In both regions, the heat budget adds up, with residuals of 0.001 W/m^2 (SPG) and 0.0002 W/m^2 (tropical region).

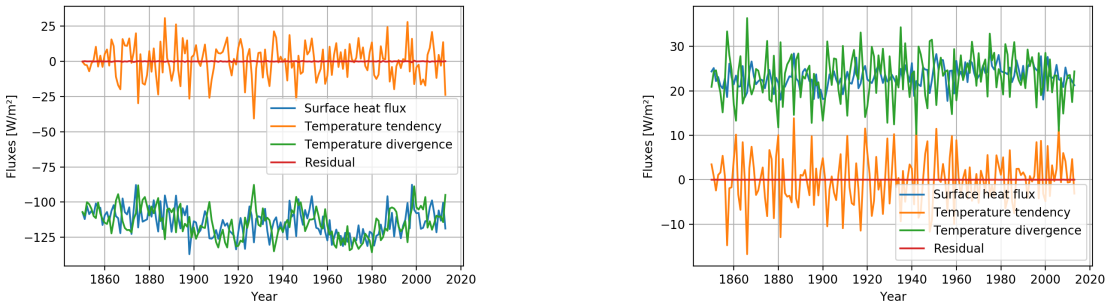

(a) Total heat budget in the SPG

(b) Total heat budget in the tropical region

Figure 4.14: Total annual heat budget [W/m^2], with vertically integrated heat divergence (green), vertically integrated heat tendency (orange), surface heat flux (blue) and residual (red), in the SPG (left) and the tropical region (right), for the first member of the ensemble run, 1850-2014.

4.4.2 Temperature tendency

Fig. 4.15a shows TEND in the SPG region from 1850 to 2014, for the first member of the ensemble run. There are large interannual variations, and there are several periods of annually alternating positive and negative values, for instance in the 1960s. The temporal average TEND over all ensemble members (ensemble mean) is 0.02 W/m^2, so there is close to no change in the average SPG temperature in this period. In the tropical region (Fig. 4.15b) the amplitude of the TEND is lower, about half of the amplitude in the SPG. Still, the pattern of alternating positive and negative values is similar, and the 1850-2014 average of TEND in the tropical region is close to zero (-0.01 W/m^2).

Both the SPG and the tropical region have close to no TEND in the 164 year average, but the 1970-2014 TEND is different. The SPG has a 1970-2014 average of -0.38 W/m^2, a cooling, in opposition of what one could expect during times of global warming. This negative trend could be related to the substantial decrease in AMOC strength at 26.5°N after 1975, presented in Fig. 4.16. This corresponds well with earlier studies on AMOC strength and SST variability [Schmith et al., 2014, Zhang et al., 2019]. The tropical region has an average TEND of 0.89 W/m^2, a warming in the order of the anthropogenic warming in this period (of about 1 W/m^2). The cooling in the SPG and heating the tropical region is present across all members.

Fig. 4.1a and 4.2a showed a SST cooling in the SPG, and a heating in the tropics. The average TEND over 1970-2014 showed the same pattern: decreasing temperatures in the SPG, and increas-

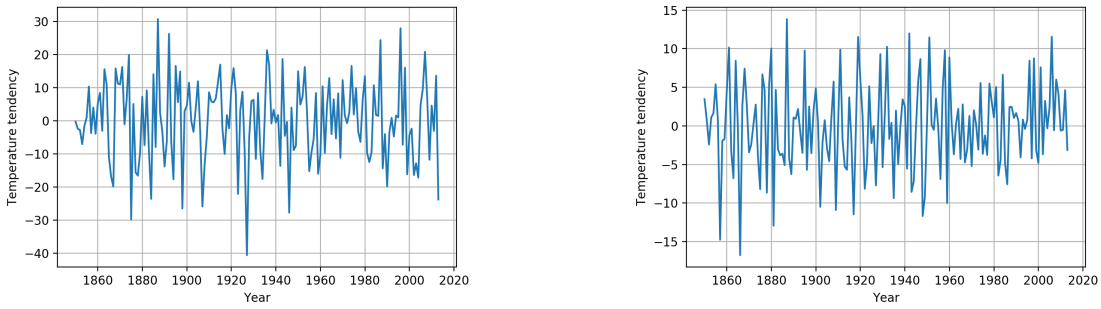

(a) TEND in the SPG

(b) TEND in the tropical region

Figure 4.15: Vertically integrated annual temperature tendency in the SPG (left) and the tropical region (right), illustrated with the first ensemble member, 1850-2014.

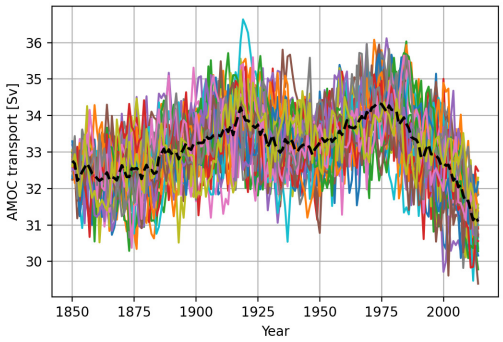

Figure 4.16: Annual mean of AMOC transport at 26.5°N, with all members (in colors) and ensemble mean (dashed, black), from 1850-2014.

ing ones in the tropical region. Despite the relatively low correlations between SST and TEND in the tropical region (Fig. 4.13), this heating trend is present in both SST and TEND.

4.4.3 Temperature divergence

The DIV represents the ocean dynamics effects in the heat budget. The DIV in the SPG and the tropical region for the first ensemble member is shown in Fig. 4.17. In the SPG (Fig. 4.17a) the DIV is negative or, more precisely, there is a temperature convergence. This convergence, originating from the ocean circulation, acts to heat the SPG. The tropical region has positive DIV (Fig. 4.17b), and is losing heat to the surrounding ocean. The variability here seems to have a higher frequency than in the SPG, and the amplitude is about half of the amplitude in the SPG.

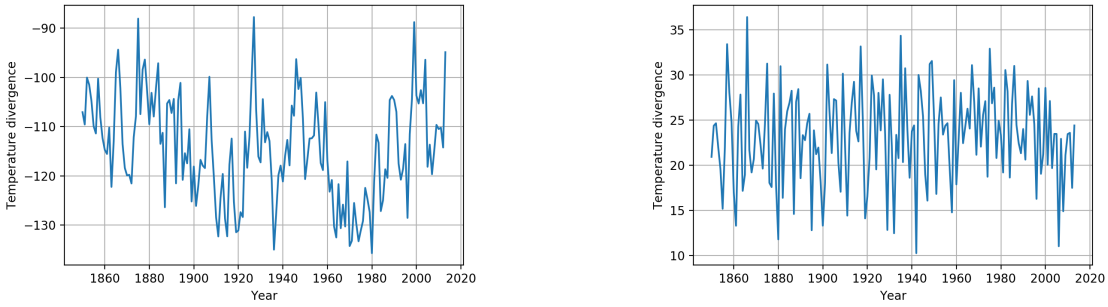

(a) DIV in the SPG

(b) DIV in the tropical region

Figure 4.17: Vertically integrated annual temperature divergence in the SPG (left) and the tropical region (right), for the first member of the ensemble run, 1850-2014.

TEND and DIV have a negative correlation over the whole North Atlantic, and this is presented in Fig. 4.18a. Hence, a positive TEND, heating, correlates with a negative DIV, or convergence. In the eastern part of the SPG, especially for longer time scales, the correlation is not that strong. This is contradictory to the expected result, that the correlation between TEND and DIV is stronger on longer time scales. There could be other interferences, making the relation between heating and convergence (or cooling and divergence) weaker, as for instance influence from the heat flux.

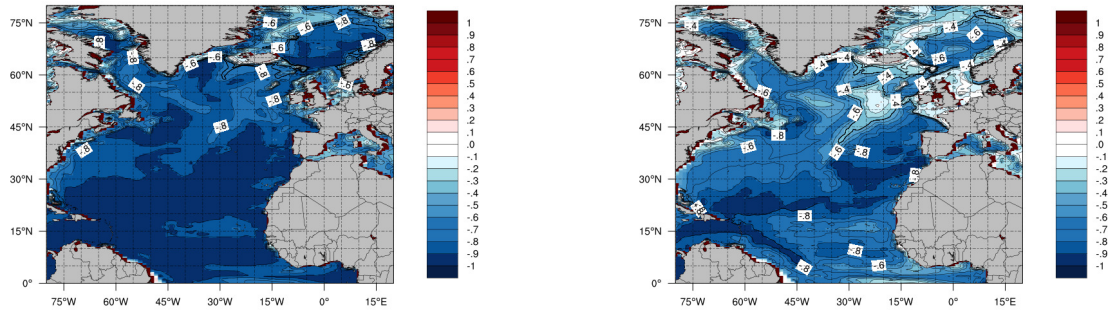

(a) DIV and TEND, unfiltered

(b) DIV and TEND, filtered

Figure 4.18: Correlation map for full period (1850-2014), annual DIV and TEND. The correlation maps are computed for each member, and then the correlation maps are averaged. The filter is a 10 years low-pass filter.

4.4.4 Surface heat flux

The HFLX is calculated only at the surface, and no vertical integration is needed. Fig. 4.19 shows the HFLX in the SPG (4.19a) and the tropical region (4.19b), for the first member. As for the temperature divergence, the two regions have opposite signs. In the SPG, the ocean is on average warmer than the atmosphere, and the ocean loses heat to the atmosphere (negative HFLX). In the tropics, the ocean is on average gaining heat from the atmosphere (positive HFLX).

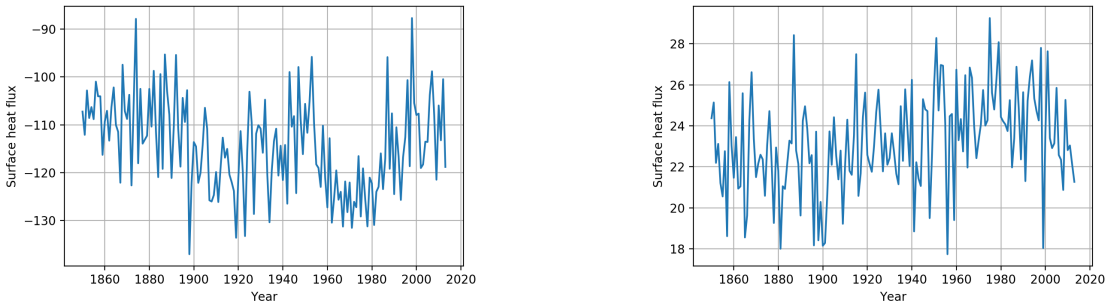

(a) HFLX in the SPG

(b) HFLX in the tropical region

Figure 4.19: Annual surface heat flux in the SPG (left) and the tropical region (right), for the first member of the ensemble run, 1850-2014.

The correlation between TEND and HFLX on an interannual time scale, presented in Fig. **??**, shows a positive correlation over most of the North Atlantic. That is, an increase in HFLX and an increase in TEND happens simultaneously. However, this correlation is not consistent on longer time scales (Fig. 4.20b), where most of the North Atlantic has correlations near 0. It looks like the HFLX has a possible interannual impact on TEND in the SPG (with a maximum of 0.6), but little direct influence on a longer time scale. In the tropical region the interannual correlation between HFLX and TEND is lower (maximum 0.4).

As the heat budget only includes TEND, HFLX and DIV, one could expect the correlation maps between TEND and HFLX and TEND and DIV to add up to 1. This is not the case, however. A possible explanation is presented in Fig. 4.21, that shows a strong correlation between DIV and HFLX on a decadal time scale. The correlation reaches a maximum of 0.9 in the eastern part of the SPG region, where the DIV-TEND correlation is particularly low. The HFLX-DIV correlation on decadal time scales corresponds well with several earlier studies [Gulev et al., 2013, Peings and Magnusdottir, 2014].

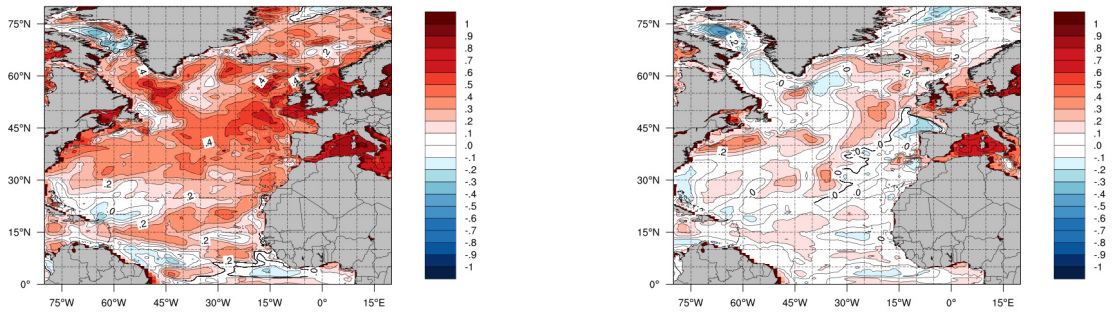

(a) HFLX and TEND, unfiltered

(b) HFLX and TEND, filtered

Figure 4.20: Correlation map for full period (1850-2014), annual HFLX and TEND. The correlation maps are computed for each member, and then the correlation maps are averaged. The filter is a 10 years low-pass filter.

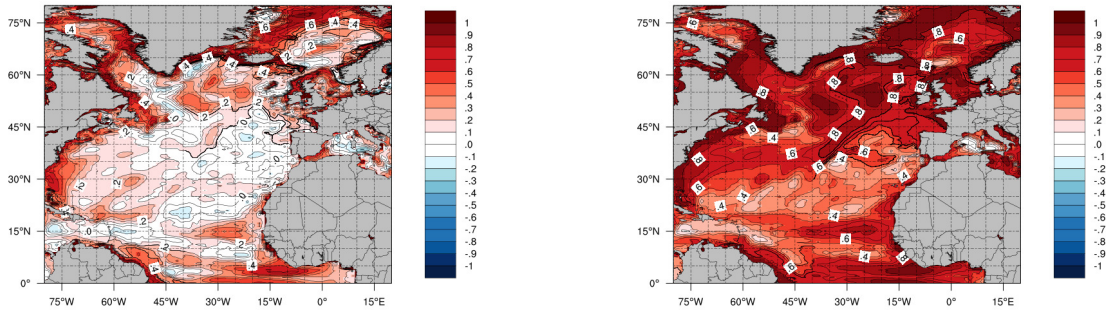

(a) HFLX and DIV, unfiltered

(b) HFLX and DIV, filtered

Figure 4.21: Correlation map for full period (1850-2014), annual HFLX and DIV. The correlation maps are computed for each member, and then the correlation maps are averaged. The filter is a 10 years low-pass filter.

4.4.5 The heat budget in the mixed layer

The heat budget analysis can be extended to separate between surface and deep ocean, in order to obtain a more accurate representation of the surface variability. Fig. 4.22 shows the box averaged heat budget for the mixed layer, defined as the upper 62.5m of the ocean (the first 5 z-levels in the model output), in the SPG (Fig. 4.22a) and the tropical region (Fig. 4.22b). Note that the mixed layer depth varies with latitude and season, and this is an approximation. The residual is now representing the exchange of heat between the mixed layer and the deeper ocean. A positive (negative) residual reflects a gain (loss) of heat from the deeper ocean to the surface layer. In the SPG, the HFLX and the residual are in anti phase; a loss of heat at the surface is balanced by a gain to the mixed layer from the deeper ocean. In the tropical region, there are indications that the mixed layer DIV plays a larger role, being in phase with the residual. A larger DIV is balanced by a positive residual, heating the mixed layer from below. While the residual in the SPG is larger than the residual in the tropical region, the amplitudes are of the same magnitude.

The average residual for the first ensemble member is 8.9 W/m^2 in the tropical region, compared to 87.8 W/m^2 in the SPG, an order of magnitude in difference. There is a higher total vertical heat transport at 62.5m in the SPG than in the tropical region. In the tropical region, TEND is positively related with the residual. This could imply that TEND variations in the mixed layer in part are driven by heating from the deeper ocean.

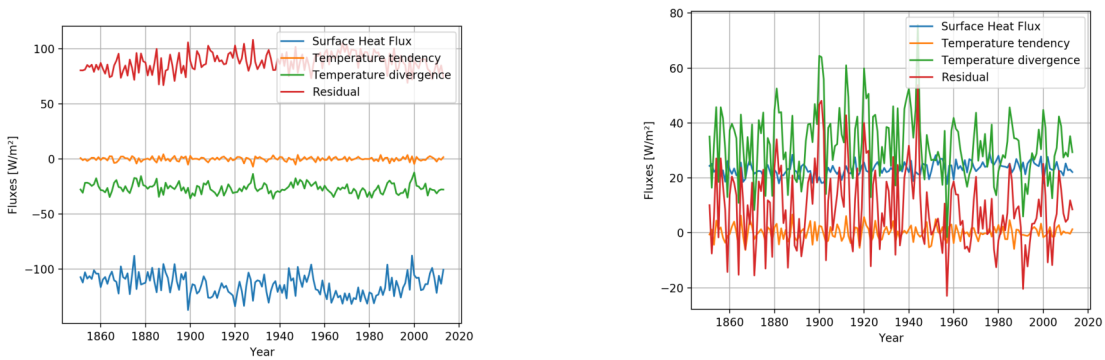

(a) Mixed layer heat budget in SPG

(b) Mixed layer heat budget in the tropical region

Figure 4.22: Annual heat budget for the mixed layer, with vertically integrated heat divergence (green), vertically integrated heat tendency (orange), surface heat flux (blue) and residual (red), in the SPG (left) and the tropical region (right), for the first member of the ensemble run, 1850-2014.

4.5 The multiple linear regression model

As explained in section 3.1.3, multiple linear regression (MLR) can be used to study the combined influence of two variables on one phenomenon, and to investigate their relative importance. In this

case, I used multiple regression analysis to estimate the impact of DIV and HFLX on TEND, and AMOC and NAO on TEND, in the SPG and the tropical region. A summary of the results from the MLR model is given in Table 4.1 (subsection 4.5.5). First, I ran the MLR on the heat budget components, DIV and HFLX for the whole North Atlantic. This run is both a verification for the heat budget and the MLR model.

4.5.1 The MLR model and the heat budget

The MLR model ran with the heat budget components in the North Atlantic produces Eq. 4.2. The equation is nearly identical to Eq. 2.1, and the MLR explains on average (over all ensemble members) 99.9 % of the variance in TEND. The small deviation from 100 % might be related to for instance the simplification by using constant density.

$$y_{reg} = 1.001 \cdot HFLX - 1.005 \cdot DIV \tag{4.2}$$

Fig. 4.23 is a visualization of the accuracy of the MLR ran with the heat budget components. The regressed function (orange, dotted) is closely following the TEND (blue), explaining nearly all of the variance.

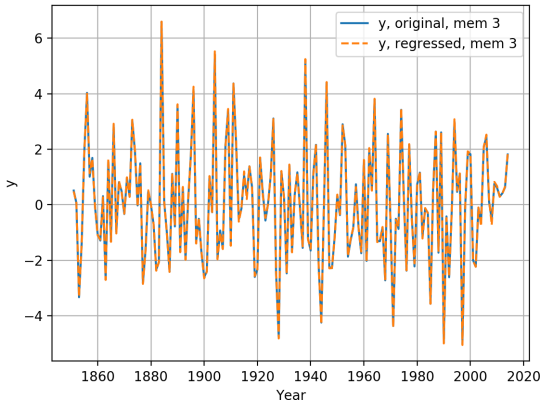

Figure 4.23: The linear regression model run (dotted, orange) with DIV and HFLX, compared to TEND (blue) for the third ensemble member.

The correlations between the components show that HFLX might have a slightly stronger influence on TEND (with a correlation of 0.698) than the impact of DIV on TEND (correlation of -0.615). The sum of the individual correlations squared is 0.870, indicating that the components together would explain 87.0 % of the variance in TEND, if the two predictors were uncorrelated.

The averaged (over all ensemble members) variance explained from the MLR model is 99.9 %. It looks like the MLR is explaining more than the sum of the individual simple regressions, probably due to the correlation between the two predictors, as illustrated in section 4.4.4.

4.5.2 AMOC and NAO in the MLR model

In the last section, we saw that close to 100% of the TEND in the North Atlantic can be explained by applying the MLR model on the heat budget components. This result is the combination of the ocean dynamics and the thermodynamic forcing from the atmosphere. To investigate the relative importance of the dynamics and thermodynamics, the upcoming subsections will present the MLR model with individual influences of DIV and HFLX, as well as AMOC and NAO. Fig. 4.24a and 4.24b present time series of modelled (orange) and observed (blue) AMOC and NAO, defined as in subsection 3.1.3.

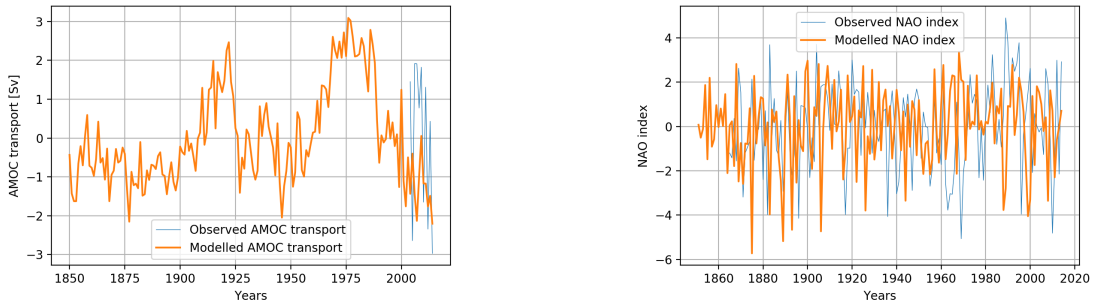

(a) AMOC anomaly, [SV]

(b) NAO index anomaly

Figure 4.24: The two components in the multiple regression analysis; annual anomalies (deviation from ensemble mean) of AMOC and NAO, from the first ensemble member of the model (orange) and observed (blue). The observations are included to show that the model variability is reasonable.

The correlation maps are giving an impression of the spatial relations between TEND, AMOC and NAO. Fig. 4.25 shows the correlation between AMOC and TEND. There is a rather low correlation between AMOC and TEND in the whole North Atlantic on an annual scale (Fig. 4.25a), with a maximum in the west of the SPG. Thus, in the presence of interannual variability, AMOC seems to have relatively little impact on TEND. The filtered data (Fig. 4.25b) has a higher correlation, especially in the SPG. The NAO on the other hand, has a higher correlation with TEND on an interannual time scale (Fig. 4.26a) than on a decadal time scale (Fig. 4.26b). The NAO and TEND correlation is strongest on an interannual time scale in the SPG, with a maximum correlation of 0.5.

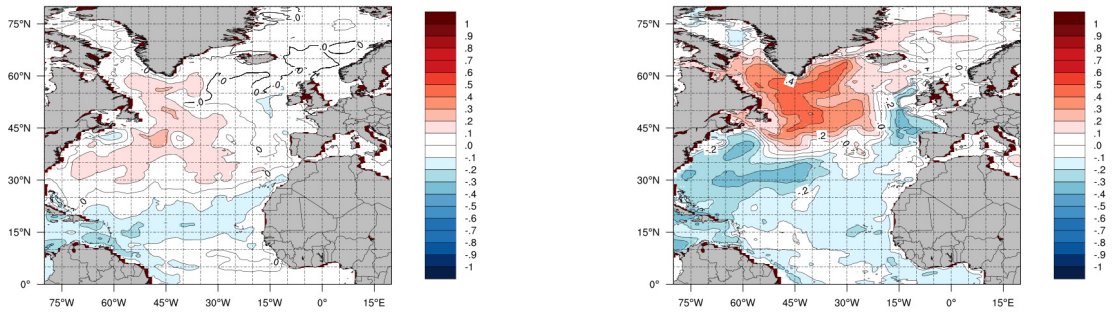

(a) AMOC and TEND, unfiltered

(b) AMOC and TEND, filtered

Figure 4.25: Correlation map for AMOC and TEND (1850-2014). The correlation maps are computed for each member, before the correlation maps are averaged. The filter is a 10 years low-pass filter.

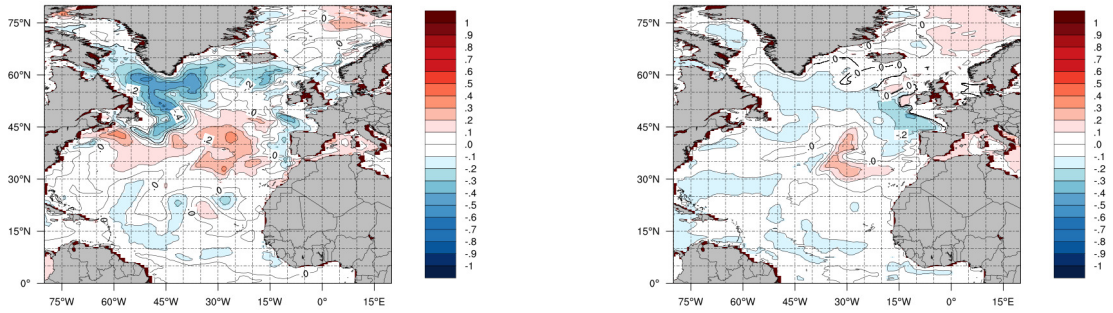

(a) NAO and TEND, unfiltered

(b) NAO and TEND, filtered

Figure 4.26: Correlation map for NAO and TEND (1850-2014). NAO is averaged over boreal winter (Dec-Mar), and TEND over a calender year. The correlation maps are computed for each member, before the correlation maps are averaged. The filter is a 10 years low-pass filter.

4.5.3 The MLR model in the subpolar gyre

The multiple linear regression (MLR) ran in the SPG with AMOC and NAO as predictors, results in Eq. 4.3:

$$y_{reg} = -3.158 W/m^2 \cdot x_1 + 2.213 J/m^5 \cdot x_2 \tag{4.3}$$

where x_1 is the NAO index, and x_2 is the AMOC strength at 26.5°N. The regression coefficients, c_1 and c_2, are averages of all ensemble members. The units of the regression coefficients, W/m^2 and J/m^5 comes from the calculations of c_1 and c_2, and convert all terms to the unit W/m^2. Fig. 4.27 shows the MLR for two of the members, 3 and 15, in the ensemble run. A visual inspection of the runs reveals that the MLR catches the general pattern of the TEND, but that the amplitude is underestimated.

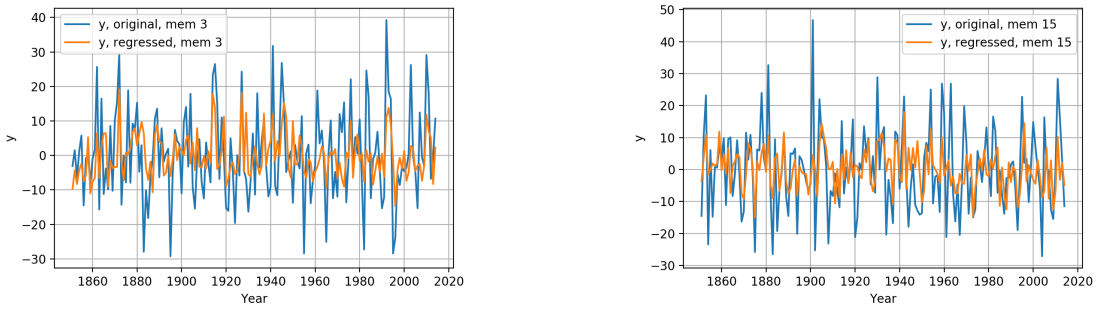

(a) MLR, member 3

(b) MLR, member 15

Figure 4.27: The result of the MLR (orange) in the SPG, ran with AMOC and NAO, compared to the original TEND (blue), y, for two members.

The mean NAO-TEND correlation over all 30 members for 1850-2014, is -0.421. The negative correlation between NAO and TEND indicates that an anomalously high TEND coincides with a low NAO index (smaller difference between the pressure over the Azores and Iceland). For AMOC and TEND, the mean correlation is 0.101, a negligible correlation. Hence, on an interannual time scale, NAO seemingly has a higher correlation with TEND in the SPG than AMOC.

A total of 20.5 % of the variance in TEND is explained from this MLR model. The correlation coefficients squared estimate the relative contributions of the two components. As NAO and TEND has $r^2 = 0.180$, and AMOC and TEND has $r^2 = 0.015$, the sum is 0.195, corresponding to a variance explained of 19.5 %. Interestingly, this indicates a total variance explained about 1% lower than the MLR. The combination of the two variables seems to have a larger effect than the individual influence, similarily to the DIV and HFLX in the MLR run on the heat budget. However, 1% is small compared to the interquartile range of 17.5 - 23.7 % of the variance estimates derived from the individual members.

To assess the relative importance of NAO and AMOC on TEND, I ran the MLR model with the two components individually. More specifically, I set $c_1 = 0$ to look at the individual contribution

of AMOC (x_2), and $c_2 = 0$ to look at NAO (x_1) only. Fig. 4.28 shows the MLR ran with AMOC only (Fig. 4.28a) and NAO only (Fig. 4.28b). For a reference, the MLR is run with DIV and HFLX only, as an "upper limit" of how much the dynamics and thermodynamics can explain.

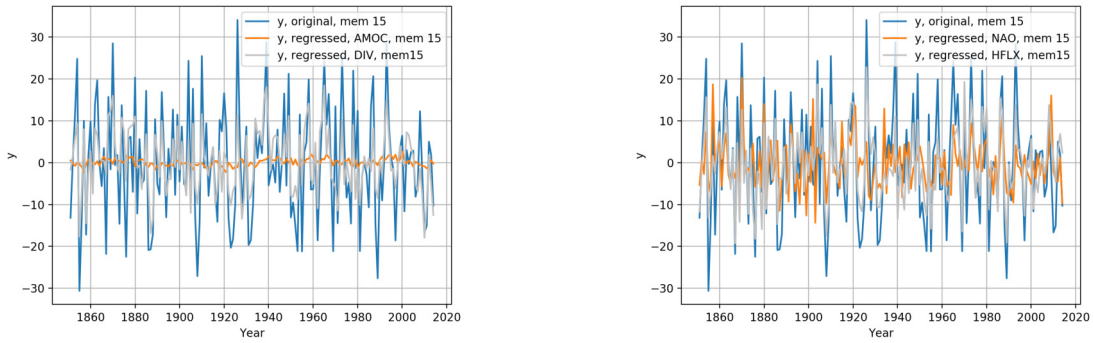

(a) MLR run with AMOC only

(b) MLR run with NAO only

Figure 4.28: The TEND (blue) and the MLR (orange) for member 15 in the SPG, ran with AMOC (left) and NAO (right) only, including DIV (left) and HFLX (right) (grey) as upper limits for variance explained.

Both visually and from correlations, it is evident that NAO has a stronger relation to TEND than AMOC's relation with TEND, on an interannual time scale. The heat budget components, DIV and HFLX (in grey), are individually explaining 55.3% and 54.8% of the TEND variance in the SPG, from the MLR runs. The MLR model with NAO alone explains 18.0%, while AMOC only explains 1.2%. Hence, NAO represents a substantial part of the thermodynamics on an interannual time scale, while AMOC explains very little of the ocean dynamics. Using a 10 year low-pass filter, the result is quite different, with a variance explained of 34.8%. The filtered MLR with both AMOC and NAO is presented in Eq. 4.4 and Fig. 4.29.

$$y_{reg} = -2.658 W/m^2 \cdot x_1 + 4.307 J/m^5 \cdot x_2 \tag{4.4}$$

The absolute value of the average correlation coefficients are more or less flipped from the unfiltered to the filtered run, with a NAO-TEND correlation of -0.155, and an AMOC-TEND correlation of 0.466. On a decadal time scale, the ocean circulation seemingly plays a larger role than the thermodynamics. The individual contribution (obtained by putting c_1 and c_2 separately to zero) from AMOC and NAO are visualized in Fig. 4.30. The filtered MLR model with NAO is explaining 1.2%, while AMOC alone explains 21.1%, about 20 times more than NAO. In total, 34.8% is explained from MLR in the SPG, so the remaining part of the variance explained by the filtered MLR model (34.8% - 1.2% - 21.1% = 12.5 %), is explained by the combined effect of NAO and AMOC (e.g., due to cancellation of variability unrelated to TEND). However, some of the variance explained by AMOC only, may also be influenced by NAO. This aspect will be further discussed in the Discussion

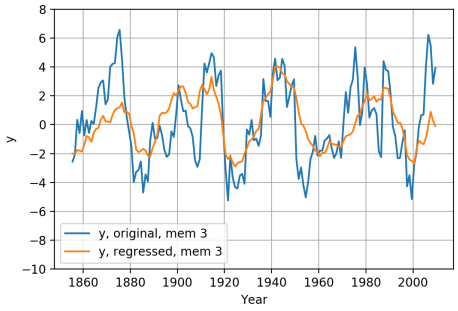

(a) Filtered MLR, member 3

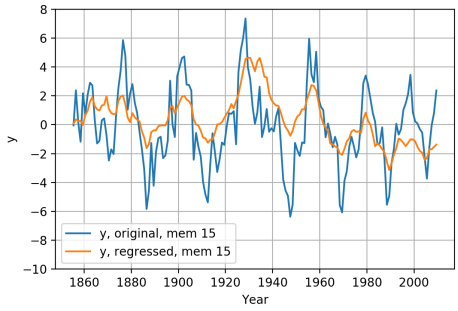

(b) Filtered MLR, member 15

Figure 4.29: The filtered multiple linear regression (orange) in the SPG, ran with AMOC and NAO, compared to the original temperature tendency (blue), y, for two members. The filter is a 10 years low-pass filter.

chapter.

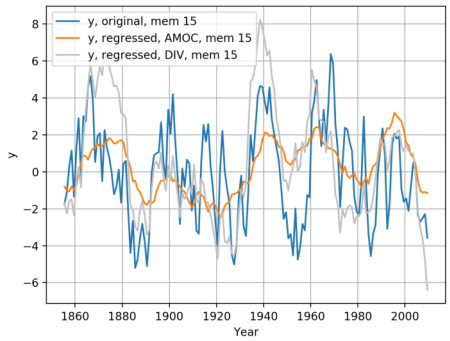

(a) MLR ran with AMOC only

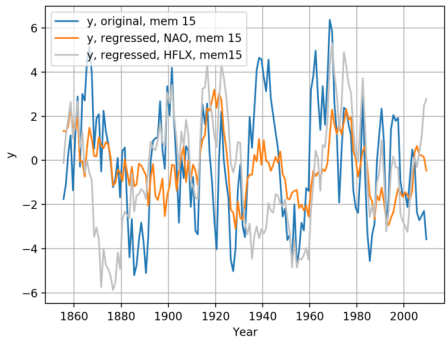

(b) MLR ran with NAO only

Figure 4.30: The 10 years low-pass filtered TEND (blue) and the MLR (orange) for member 15 in the SPG, with AMOC (left) and NAO (right) only. DIV (left) and HFLX (right) (grey) are included as upper limits for variance explained.

4.5.4 The MLR model in the tropical region

In the tropical region, there is in general a lower variance explained than in the SPG. Running the MLR model with AMOC and NAO as predictors in the tropical region results in Eq. 4.5 and Fig. 4.31. The mean of the variance explained over all members is 6.5%, a small percentage.

$$y_{reg} = -0.293W/m^2 \cdot x_1 - 1.528J/m^5 \cdot x_2 \tag{4.5}$$

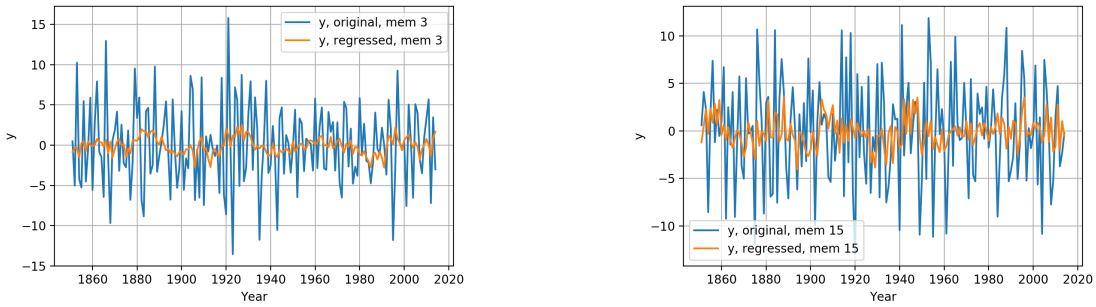

(a) MLR, member 3

(b) MLR, member 15

Figure 4.31: The result of the multiple linear regression (orange) in the tropical region, using AMOC and NAO as predictors, compared to the original TEND (blue), y, for two members.

The average correlation between annual NAO and TEND in the tropical region is -0.112, several times lower than in the SPG. For AMOC and TEND the estimated correlation is -0.223 on an annual time scale, higher than in the SPG. The negative correlation indicate that a positive NAO index, and an anomalously strong AMOC is correlated with a negative TEND, a cooling. The correlations squared sum to an average of 0.069 in the tropical region, indicating that the NAO and AMOC can explain 6.9 % of the TEND variance in the tropical region. This is somewhat higher than the variance explained by the MLR model; the variance explained by the individual components is higher than the combined result. Hence, there could be some correlation between NAO and AMOC in the tropical region, that gives an overlap in explaining TEND.

As for the SPG, I ran the MLR model with the individual components in the tropical region, and this is presented in Fig. 4.32. In difference to the SPG, the DIV and HFLX are having quite different impacts on TEND in the tropical region. While DIV alone is explaining 84.0 % of the variance in TEND, HFLX only explains 12.8%. This indicates that the ocean plays a substantial role in the interannual TEND variance in the tropical region. Neither AMOC or NAO explain much of the TEND variance, only 5.2 and 1.6 %, respectively.

Running the MLR model with a 10 year low-pass filter in the tropical regions produces Eq. 4.6 and Fig. 4.33. The filtered MLR explains 9.6 % of the TEND variance, somewhat higher than the unfiltered, but still rather small. It seems like the MLR model does not work well in the tropics, using AMOC and NAO to model TEND. The filtered NAO and TEND has a correlation of -0.161, and AMOC and TEND has a correlation of -0.257. As for the unfiltered run, the sum of the correlations squared are slightly higher than variance explained by the full MLR model, but still within the interquartile range. NAO alone explains 2.2 %, and AMOC alone explains 7.6 % of the variance in TEND, summing to 9.8 %. Fig. 4.34 is showing the same result; it is clear the the MLR model

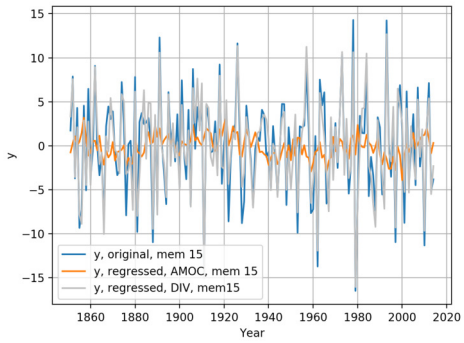

(a) MLR ran with AMOC only

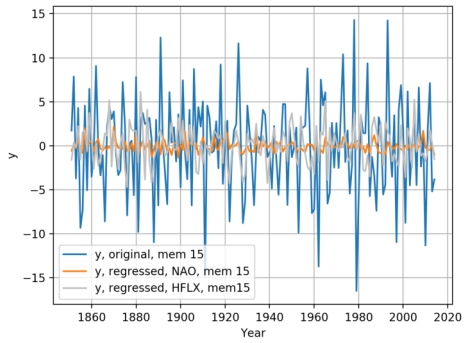

(b) MLR ran with NAO only

Figure 4.32: The TEND (blue) and the multiple linear regression (orange) for member 15 in the tropical region, ran on AMOC (left) and NAO (right) only, with DIV (left) and HFLX (right) (grey) as upper limits for variance explained.

is not explaining much of the TEND with either NAO or AMOC.

$$y_{reg} = -0.244W/m^2 \cdot x_1 + 0.104J/m^5 \cdot x_2 \tag{4.6}$$

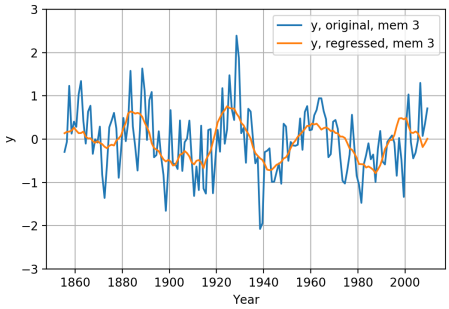

(a) Filtered MLR, member 3

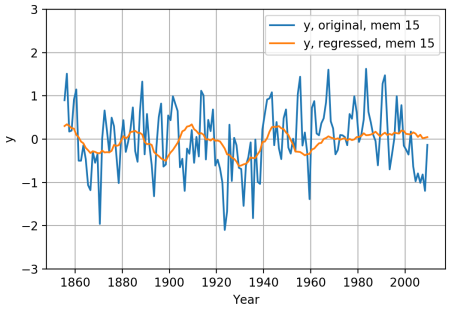

(b) Filtered MLR member 15

Figure 4.33: The filtered result of the multiple linear regression (orange) in the tropical region, ran with AMOC and NAO, compared to the original temperature tendency (blue), y, for two members. The filter is a 10 years low-pass filter.

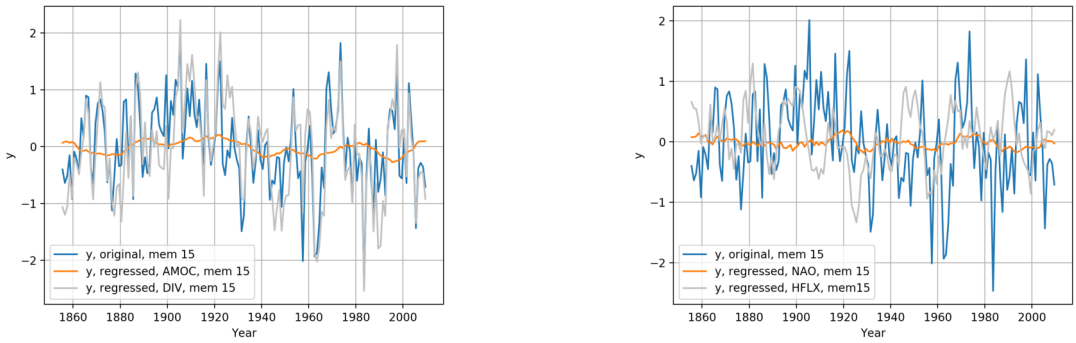

(a) MLR ran with AMOC only

(b) MLR ran with NAO only

Figure 4.34: The 10 years low-pass filtered TEND (blue) and the MLR (orange) for member 15 in the tropical region, ran with AMOC (left) and NAO (right) only. DIV (left) and HFLX (right) (grey) are included as upper limits for variance explained.

4.5.5 A summary of the MLR model

Table 4.1 gives a summary of the MLR runs in the SPG and the tropical region, on both the heat budget components, AMOC and NAO. To give an impression of the uncertainty in the runs, the 25th and 75th percentiles are included. The largest uncertainties are found in the filtered results, due to the spreading results in members produced by the filter.

The largest variance explained by the MLR model, 34.8 %, is found in the SPG on a decadal time scale. Most of this variance explained comes from AMOC, which individually explains 21.1 % of the variance in TEND in the SPG. At its best, the MLR model run with AMOC and NAO explains about one third of the variance in TEND. In the tropical region, NAO and AMOC explains very little of the TEND variance. This could be described as a modest result. How the MLR model could be improved, will be presented in the Discussion.

Table 4.1: Overview of the multiple linear regression runs, correlations and variance explained in the SPG and the tropical region. The correlation coefficients are squared and averaged over all ensemble members. The 25th and 75th percentiles are given in the squared brackets.

	Subpolar gyre		**Tropical region**	
	Unfiltered	Filtered	Unfiltered	Filtered
Regression equation, MLR with NAO and AMOC	y_{reg} = - 3.158 $W/m^2 \cdot x_1$ + 2.213 $J/m^5 \cdot x_2$	y_{reg} = - 2.658 $W/m^2 \cdot x_1$ + 4.307 $J/m^5 \cdot x_2$	y_{reg} = - 0.293 $W/m^2 \cdot x_1$ - 1.528 $J/m^5 \cdot x_2$	y_{reg} = - 0.244 $W/m^2 \cdot x_1$ + 0.104 $J/m^5 \cdot x_2$
r^2, HFLX and TEND	0.557 [0.516 0.595]	0.037 [0.001 0.048]	0.136 [0.100 0.163]	0.018 [0.004 0.171]
r^2, DIV and TEND	0.563 [0.535 0.594]	0.483 [0.415 0.536]	0.842 [0.829 0.857]	0.564 [0.515 0.620]
r^2, NAO and TEND	0.180 [0.140 0.205]	0.060 [0.009 0.075]	0.017 [0.005 0.023]	0.033 [0.013 0.046]
r^2, AMOC and TEND	0.015 [0.002 0.021]	0.231 [0.153 0.310]	0.052 [0.041 0.064]	0.078 [0.033 0.121]
variance explained by MLR with NAO and AMOC	20.5 [17.5 23.7] %	34.8 [28.6 42.4] %	6.5 [4.5 8.3] %	9.6 [5.7 13.6] %

5. Discussion

In this discussion, I will look at possible interpretations, restrictions and improvements of the models, as well as the external forcing and predictability.

5.1 The model and observations

In the Results, the observed SST, HFLX, NAO and AMOC were presented along with the modelled variables. In which area is NorESM accurately modelling the real world, and where are the simulations not so good?

Table 5.1 gives a summary of the standard deviation (std) and mean value for observations and the first member of the NorESM ensemble run in the SPG and the tropical region. The std and mean values are calculated over the period of available observations, all on an annual time scale (see Table 4.1 in the Methods section for an overview of observations). The model shows some agreement with observations, but in some regions and for some variables, one has to be particularly careful in making interpretations from the model. There is for instance a large deviation between observed and modelled AMOC, both in mean and standard deviation. NorESM is overestimating the strength of AMOC, and underestimating the variance (std squared). This may for instance influence the MLR model, as the role of AMOC might be larger with a higher variance (closer to observed AMOC). Still, the short period of observations of AMOC makes the assessment of the model more uncertain. The underestimation of AMOC variability is a known bias of several models [Wang et al., 2014, Zhang et al., 2019, Yan et al., 2018], as mentioned in the Theory (section 2.5). Also, the SST is overestimated in the SPG, and underestimated in the tropical region, by over 1°C.

One of my objectives for this thesis, is to look at the low-frequency variability in NorESM and the observations. In section 4.2, I presented the power spectrum for the modelled and the observed SST. On average, the period of the maximum power of the low-frequency variability in the SPG, was 20-60 years, compared to 80 years in the observations. The variability in the model has a higher frequency than the observations. A spread in the models and the observations is also found in several other studies, as discussed in section 2.8. These inconsistencies could for instance come from the errors in modelling SST (underestimated variance and over 1°C error in mean) and AMOC (underestimated variance and overestimated mean), or other modelling errors. Also, the rather short range of observations makes the uncertainty large, and the modelled average SST power spectrum is still between the 90th percentile of the observed red spectrum.

Table 5.1: Overview of the standard deviation (std) and mean of observations and the first member of the NorESM ensemble run, including SST, HFLX, NAO and AMOC. The std and mean are calculated from annual data. As NAO is defined as normalized pressure difference, and AMOC is calculated at 26.5°N only, they are the same in all of the North Atlantic (same values in SPG and tropical region).

	Subpolar gyre		**Tropical region**	
	Observations	Model	Observations	Model
std, SST [°C]	0.36	0.26	0.39	0.23
mean, SST [°C]	7.45	8.82	25.41	23.35
std, HFLX [W/m^2]	7.14	9.68	6.22	2.36
mean, HFLX [W/m^2]	- 22.84	- 114.22	48.36	23.21
std, NAO [ ]	1.96	1.81	1.96	1.81
mean, NAO [ ]	0.18	0.00	0.18	0.00
std, AMOC [Sv]	1.89	0.64	1.89	0.64
mean, AMOC [Sv]	18.89	31.97	18.89	31.97

Both the model and the observations indicated a low-frequency internal variability in the SPG, but not in the tropical region. What could be the explanation for this? One possible reason could be a limited understanding of the mechanisms driving climate variability in low-latitudes. For instance, the link between the tropical SST and SPG SST might be stronger than modelled in NorESM. Another possible explanation could be that the external forcing plays a larger role in the tropical region than in the SPG. The modest results from the MLR model with AMOC and NAO in the tropical region could also be an indication of external forcing being more important. This is also the conclusion of several studies on external forcing, see section 2.6. The role of the external forcing will be discussed in the next section.

5.2 Externally forced variability

The focus of this thesis has been the internal variability, estimated as the deviation from the ensemble mean. As presented in the Theory section, some studies indicate that external forcing is driving the AMV, but is this the case in NorESM? Fig. 5.1 shows the correlation map between the vertically integrated temperature tendency (TEND) and the ensemble mean (external variability) of TEND. There is little correlation between the externally forced variability and the total signal on an interannual time scale (Fig. 5.1a), around 0.2 for all of the North Atlantic. For the 10 years low-pass filtered data (Fig. 5.1b) the correlation is higher. The subtropical region and the eastern

part of the SPG seem to have a the largest influence from the external forcing, with a maximum correlation of 0.6.

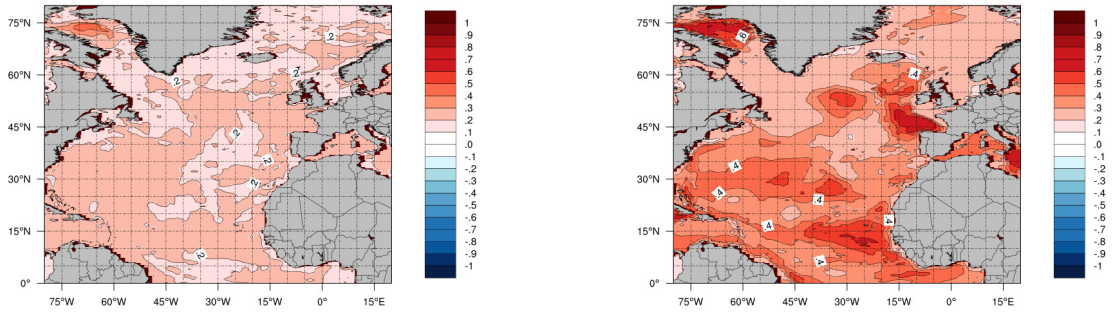

(a) External forcing and TEND, unfiltered

(b) External forcing and TEND, filtered

Figure 5.1: Correlation maps between the externally forced TEND variability and TEND, unfiltered (left) and filtered (right).

The correlation between the externally forced SST (ensemble mean) and SST (Fig. 5.2) shows a similar impact of external forcing on an interannual time scale, with a correlation of around 0.2. With the 10 years low-pass filter, the correlation is lower than for TEND. On a decadal time scale, the external forcing seemingly has a larger impact on the vertically integrated temperature tendency than the SST. One possible explanation, could be that the upper ocean is more exposed to noise than the whole column.

The studies that emphasize the external forcing, often conclude that the external forcing is crucial in the tropics, and less important in the SPG [Watanabe and Tatebe, 2019]. The correlation between externally forced TEND variability and TEND (Fig. 5.1) is higher in the tropical region than in the SPG on a decadal time scale. As the externally forced variability shows little correlation with TEND on an interannual time scale, the inclusion of the external forcing would probably not improve the MLR model remarkably. On a decadal time scale, the impact of external forcing is bigger, and it would probably have improved the MLR. There are several other modifications that might have a larger effect on the performance of the MLR model. These will be presented in the next section.

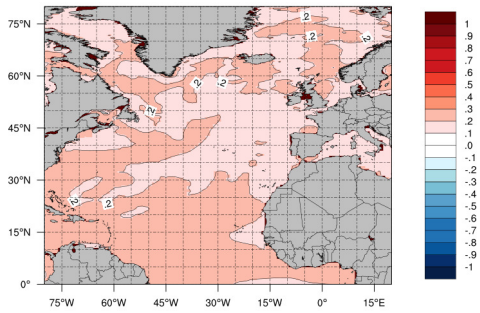

(a) External forcing and SST tendency, unfiltered

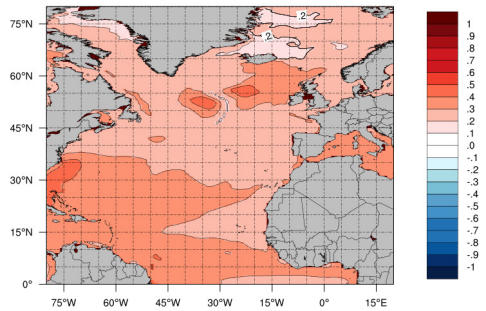

(b) External forcing and SST tendency, filtered

Figure 5.2: Correlation maps between the externally forced SST variability (ensemble mean) and SST, unfiltered (left) and filtered (right).

5.3 The MLR model

The MLR model worked very well for the heat budget, explaining nearly 100 % of the variance in TEND from DIV and HFLX. Using AMOC and NAO as predictors, the variance explained is reduced. This is an expected result, as AMOC and NAO are not explaining all of the variance in the ocean dynamics and the thermodynamic ocean-atmosphere interaction. To increase the variance explained, one would have to investigate the other patterns of atmospheric and oceanic variability that contribute to DIV and HFLX. This could be interactions between the ocean and the atmosphere, or properties of the ocean and the atmosphere, such as damping from the SPG temperature. This section presents flaws with the MLR model run with AMOC and NAO, and possible improvements.

As mentioned several times, there is an interaction between the ocean and the atmosphere, and to completely separate them is not possible. One of the interactions, is the influence of the atmosphere on AMOC. In NorESM, the correlation between NAO and AMOC in the SPG is rather low on an interannual time scale (average $r^2 = 0.006$), but stronger for HFLX and AMOC (average $r^2 = 0.064$). For the 10 years low-pass filtered data, the correlation between HFLX and AMOC is higher, with $r^2 = 0.497$ (averaged over all ensemble members). This indicates that AMOC and HFLX is strongly correlated on a decadal time scale in the SPG. Hence, assigning NAO as a representation of HFLX only, and AMOC as DIV only, is not accurate.

A factor that could improve the MLR, is the so-called "damping term". While the temperature divergence brings heat to the SPG, the HFLX cools it. But the SPG temperature itself works as a

damping term for the TEND. Including a third term, the SPG temperature, could possibly increase the variance explained by the MLR model. The regression coefficients would depend on more terms, and the derivation would be more complex.

Another improvement could be to look at the SST tendency instead of TEND (column integrated temperature tendency). I initially included the whole column for the sake of the heat budget. As the temperature divergence is integrated over depth, the heat budget can only be in balance if the temperature tendency also is depth-integrated. Running the MLR with SST tendency instead of TEND could improve the variance explained, as HFLX probably would correlate better with SST than TEND. The comparison with the heat budget would however have been complicated.

5.4 Predictability

5.4.1 Predictions from the MLR model

The NorESM historical run, the heat budget and the MLR model are not predicting future temperature changes, but analyse the past temperatures. NorCPM1, which uses NorESM as its physical model, has performed initialised decadal predictions, predicting retrospectively for 10 years with one start date per year from 1960 to present. The analysis of the initialised predictions was beyond the scope of the thesis. However, predictions from the heat budget and the MLR model could be made, based on the regression equations. How good would this prediction be?

The predictability of the TEND from the MLR model would depend on the predictability of DIV and HFLX or AMOC and NAO. The autocorrelations give an indication of the persistence in the variables. Fig. 5.3 shows the autocorrelation for the heat budget components, HFLX (Fig. 5.3a) and DIV (Fig. 5.3b) in the SPG, for the first ensemble member. As expected, HFLX has a lower autocorrelation than DIV, indicating that predictions for DIV could be more skilful than predictions for HFLX.

The autocorrelation for NAO and AMOC in the SPG for the first ensemble member are presented in Fig. 5.4. As for HFLX and DIV, the NAO has a lower autocorrelation than AMOC. However, there is a substantial difference in the strength of the autocorrelation for DIV and AMOC. As the DIV autocorrelation decreases to about 0 correlation after 5 years, AMOC still has an autocorrelation of around 0.35 until the 9 years lag. From the autocorrelations, it seems like AMOC has the largest contribution to the decadal predictions. That AMOC is important for decadal predictions, especially in the SPG, agrees with several studies on decadal predictions [Keenlyside et al., 2008, Yeager et al., 2012, Latif et al., 2004, Robson et al., 2018].

One should be careful in assigning parts of the variability to one variable, as already discussed in the 5.3. NAO can influence AMOC on longer time scales, and the strong autocorrelation of AMOC might partly be due to NAO and HFLX. AMOC could for instance be influenced by a persistent HFLX, which forces circulation changes [Visbeck et al., 2003]. The NorESM estimated correlation between AMOC and NAO is 0.06 on an interannual time scale, and 0.24 on a decadal time scale. This indicates little in-phase relation between NAO and AMOC, but cross correlations can tell more about possible lagged relations. Fig. 5.5 shows the cross correlation between AMOC

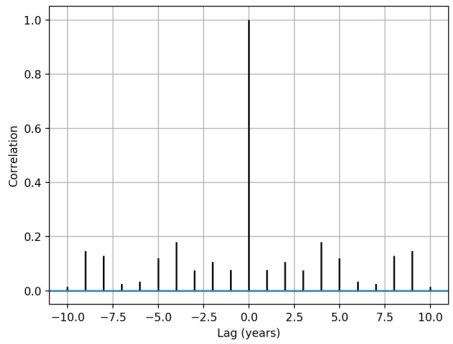

(a) Autocorrelation for annual HFLX

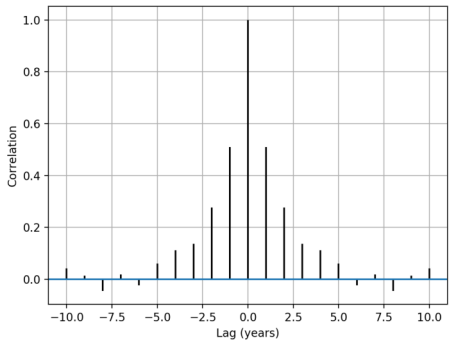

(b) Autocorrelation for annual DIV

Figure 5.3: Autocorrelation for HFLX (left) and DIV (right) in the SPG, for the first ensemble member.

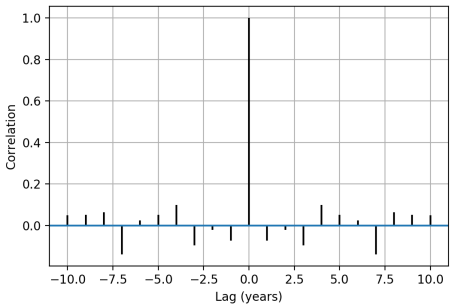

(a) Autocorrelation for annual NAO

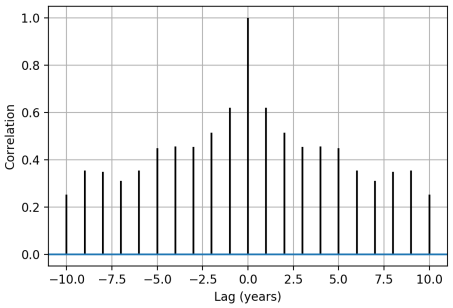

(b) Autocorrelation for annual AMOC

Figure 5.4: Autocorrelation for NAO (left) and AMOC(right), in the SPG, for the first ensemble member.

and NAO, with a maximum lag of 10 years. The strongest correlation for the unfiltered data appears with a lag of 5-6 years; that is a correlation of 0.2 between NAO and AMOC 5 years later. For the filterd data, the cross correlation is notably higher, with a maximum of 0.6 at 5 - 6 years lag.

A challenge for the MLR model predictions is the 10 years low-pass filter applied to look at longer time scales. Visually, the filter works well, as it smoothens out the variability in the time series. Unfortunately, the filter produces inconsistent results, and makes a larger spread between models than the unfiltered result. The sensitivity to this filter reduces the possibility for an accurate decadal prediction from the MLR model.

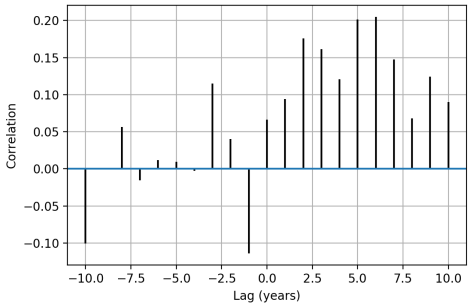

(a) Cross correlation, AMOC and NAO, unfiltered

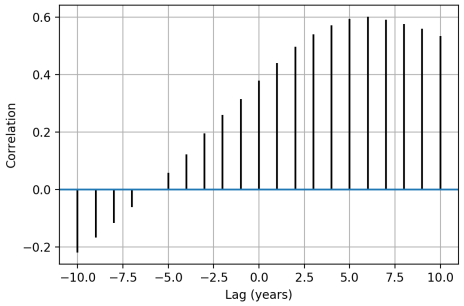

(b) Cross correlation, AMOC and NAO, filtered

Figure 5.5: Cross correlation between AMOC and NAO, unfiltered(left) and filtered (right), in the SPG for the first ensemble member. The AMOC series is lagging; year 1 gives the correlation between NAO at year 0, and AMOC at year 1.

5.4.2 NorCPM predictions in light of the MLR model

In conclusion, the MLR model would not work too well for decadal predictions. Still, in combination with the NorCPM1 predictions, the MLR model can provide useful information. NorCPM1 is a complex model, and understanding which mechanisms are driving the SST variations is not straight forward. The simplicity of the MLR model enables a simplified analysis for NorCPM1 predictions. Based on Table 4.1, I will discuss the possibility to predict TEND in the SPG with NorCPM1. The following three paragraphs will focus on predictions of TEND from DIV and AMOC, making different assumptions. The discussion is simplified by assuming no skill in HFLX and NAO, as the variance explained by HFLX and NAO is several times lower than the variance explained by DIV and AMOC on a decadal time scale.

Assuming we do not know future HFLX, but we perfectly know future DIV, how well can we expect NorCPM1 to predict SPG TEND? The heat budget showed that DIV is rather strongly correlated with TEND in the SPG, both on an interannual and a decadal time scale. With r^2(DIV,TEND) = 0.563 (interannual) and 0.483 (decadal), DIV alone could explain about 50 % of the variance in TEND, both on an interannual and a decadal time scale. A challenge is that there is no observational data of DIV, so a "perfectly known future DIV" is merely a theoretical statement.

Assuming we do not know HFLX, but we perfectly know future AMOC, how well can we expect NorCPM1 to predict SPG TEND? The correlation between AMOC and TEND indicates that AMOC can predict 1.5 % of the TEND variance on an interannual time scale (r^2(AMOC,TEND) = 0.015), and 23.1% on a decadal time scale (r^2(AMOC,TEND) = 0.231). Improving AMOC predictions would have close to no effect on an interannual time scale. For decadal predictions, the TEND predictions might be substantially improved by developing the AMOC predictions.

Assuming we do not know HFLX, but have some knowledge of future AMOC due to its autocorrelation, how well can we expect NorCPM1 to predict SPG TEND? This would make an

even smaller variance explained than from AMOC, as two predictions are combined; AMOC predicting TEND, and AMOC predicting itself. On an interannual time scale, r^2(AMOC,TEND) · r^2(AMOC,AMOC$_{lagged}$) = 0.015 · 0.6^2 = 0.005, using the autocorrelation for AMOC, with one year lag. Based on AMOC's autocorrelation and AMOC's correlation to TEND, only 0.5% of the TEND variance could be explained. On a decadal time scale, using the AMOC autocorrelation with 10 years lag, the variance explained is even less, about 0.2 % (r^2(AMOC,TEND) · r^2(AMOC,AMOC$_{lagged}$) = 0.231 · 0.3^2 =0.002).

Currently, the NorCPM1 predictions are not particularly well positioned to do skilful SPG and tropical Atlantic climate prediction. From this short analysis, improving predicitions of the heat transport (being the model output used to calculate DIV) could be a way to improve the prediction skill. Improving the AMOC predictions could also enhance the prediction skill on a decadal time scale.

6. Conclusion

To conclude this thesis, I will give a short summary of the research questions I have investigated and discussed in this thesis.

- Is there an enhanced low frequency variability in the North Atlantic SST in the historical NorESM simulations? If yes, is there a dominant period?
  - Yes and no. Yes, there is clear evidence for enhanced low-frequency in the SPG for the NorESM model run, with a an average period of 20-60 years. Robust detection of the enhanced low-frequency variability was possible through analysis of a large simulation ensemble, in difference to single simulations or observations. No, in the tropical region, there is no enhanced low-frequency variability. The average spectrum over all ensembles showed no peaks above the red spectrum.
- How is the annual column-integrated temperature tendency in the North Atlantic related to the ocean dynamics and thermodynamic atmosphere-ocean interaction? And how are these relations changing on different time scales and in different regions?
  - Averaged over the subpolar gyre, the annual mean temperature tendencies simulated in NorESM depend about equally on dynamics and thermodynamics, that is the ocean heat transport divergence and the surface heat flux (HFLX). However, the divergence plays a substantially larger role on decadal time scales, while the contribution from the surface heat flux decreases. In the tropics, the ocean heat transport divergence explains most of the temperature tendency variance on both an interannual and a decadal time scale.
- How is HFLX related to NAO, and ocean temperature divergence (DIV) related to AMOC? How much of the variance in temperature can be explained by NAO and AMOC?
  - Both the correlation of winter NAO with annual HFLX, and annual AMOC strength with annual DIV is negative in the SPG region, and close to zero in the tropical region. The NAO and HFLX has a stable correlation over time scales, while AMOC strength at 26.5°N and DIV is stronger correlated on a decadal time scale. From the MLR model in the SPG, including AMOC and NAO only, a maximum of 20.5% can be explained on interannual time scales, and 34.8 % on decadal time scales. In the tropical region, the MLR model only explained 6-7% of the TEND variance. Interestingly, the sum of the variance explained by the individual components does not add up to the variance explained by the MLR model with both components. This could be due to the correlation between the predictors.

- How well does NorESM simulate observed SST, HFLX, NAO and AMOC?
  - The model shows some agreement with observations, most of the variability in the central variables is well represented in NorESM1. However, several deviations are found between the model and the observations, especially for AMOC and SST. The model overestimates the strength of AMOC, and underestimates the variance. Also, the low-frequency SST variability has a lower period of maximum power in the model (20-60 years) than in the observations (80 years), and the mean SST is off by over 1°C in both the SPG and in the tropical region. Therefore, some cautions must be taken when generalizing these findings to the real world.

References

Jin Ba, Noel S Keenlyside, Mojib Latif, Wonsun Park, Hui Ding, Katja Lohmann, Juliette Mignot, Matthew Menary, Odd Helge Otterå, Bert Wouters, David Salas y Melia, Akira Oka, Alessio Bellucci, and Evgeny Volodin. A multi-model comparison of Atlantic multidecadal variability. *Climate Dynamics*, 43, 2014. doi: 10.1007/s00382-014-2056-1.

Mats Bentsen, Ingo Bethke, J.B. Debernard, T. Iversen, A. Kirkevåg, Ø. Seland, Helge Drange, C. Roelandt, I. A. Seierstad, C. Hoose, and J. E. Kristjánsson. The Norwegian Earth System Model , NorESM1-M – Part 1 : Description and basic evaluation of the physical climate. *Geoscientific Model Developement*, pages 687–720, 2013. doi: 10.5194/gmd-6-687-2013.

Ingo Bethke. NorCPM1 and its contribution to CMIP6 DPP. *Geoscientific Model Developement*, in prep.

Jacob Bjerknes. Atlantic Air-Sea Interaction. *Advances in Geophysics*, 10(C):1–82, 1964. ISSN 00652687. doi: 10.1016/S0065-2687(08)60005-9.

Ben B B Booth, Nick J Dunstone, Paul R Halloran, Timothy Andrews, and Nicolas Bellouin. Aerosols implicated as a prime driver of twentieth-century North Atlantic climate variability. *Nature*, 2012. ISSN 0028-0836. doi: 10.1038/nature10946.

Mark A Cane, Amy Clement, Lisa N Murphy, and Katinka Bellomo. Low-Pass Filtering , Heat Flux , and Atlantic Multidecadal Variability. *Journal of Climate*, 30:7529–7553, 2017. doi: 10.1175/JCLI-D-16-0810.1.

Amy Clement, Katinka Bellomo, Lisa N Murphy, Mark A Cane, Thorsten Mauritsen, Gaby Rädel, and Bjorn Stevens. The Atlantic Multidecadal Oscillation without a role for ocean circulation. *Science*, 2015. ISSN 10959203. doi: 10.1126/science.aab3980.

François Counillon, Noel Keenlyside, Ingo Bethke, Yiguo Wang, Mao Lin Shen, and Mats Bentsen. Flow-dependent assimilation of sea surface temperature in isopycnal coordinates with the Norwegian Climate Prediction Model. *Tellus A : Dynamic Meteorology and Oceanography*, 0870, 2016. doi: 10.3402/tellusa.v68.32437.

T. Delworth, S. Manabe, and R. J. Stouffer. Interdecadal Variations of the Themohaline Circulation in a Coupled Ocean-Atmosphere Model. *Journal of Climate*, 6, 1993.

Carsten Eden and Thomas Jung. North Atlantic Interdecadal Variability : Oceanic Response to the North Atlantic Oscillation (1865 – 1997). *Journal of Climate*, pages 676–691, 2001.

Oluwayemi A. Garuba, Jian Lu, Hansi A Singh, Fukai Liu, and Phil Rasch. On the Relative Roles of the Atmosphere and Ocean in the Atlantic Multidecadal Variability. *Geophysical Research Letters*, 45:9186–9196, 2018. doi: 10.1029/2018GL078882.

Stanley B. Goldenberg, Christopher W. Landsea, Alberto M. Mestas-Nuñez, and William M. Gray. The Recent Increase in Atlantic Hurricane Activity : Causes and Implications. *Science*, 293, 2001.

Sergey K Gulev, Mojib Latif, Noel Keenlyside, Wonsun Park, and Klaus Peter Koltermann. North Atlantic Ocean control on surface heat flux on multidecadal timescales. *Nature*, 499(7459):464–467, 2013. ISSN 0028-0836. doi: 10.1038/nature12268. URL `http://dx.doi.org/10.1038/nature12268`.

K. Hasselmann. Stochastic climate models Part I . Theory. *Tellus*, 28(6):473–485, 1976.

James W Hurrell, Yochanan Kushnir, Geir Ottersen, and Martin Visbeck. An overview of the North Atlantic Oscillation. *American Association for the Advancement of Science*, 291(5504), 2003. doi: 10.1126/science.1058761.

N S Keenlyside, M Latif, J Jungclaus, L Kornblueh, and E Roeckner. Advancing decadal-scale climate prediction in the North Atlantic sector. *Nature*, 453, 2008. doi: 10.1038/nature06921.

Noel S Keenlyside and Jin Ba. Prospects for decadal climate prediction. *WIREs Climate Change*, 7(Figure 1), 2010. doi: 10.1002/wcc.69.

Noel S. Keenlyside, Jin Ba, Jennifer Mecking, Nour-Eddine Omrani, Mojib Latif, Rong Zhang, and Rym Msadek. North Atlantic Multidecadal variability - mechanisms and predictability. In Chih-Pei Chang, editor, *Climate Change: Multidecadal and Beyond*, chapter 9, pages 141–157. World Scientific, 2015. doi: 10.1142/9789814579933_0009.

Jeff R Knight, Robert J Allan, Chris K Folland, Michael Vellinga, and Michael E Mann. A signature of persistent natural thermohaline circulation cycles in observed climate. *Geophysical Research Letters*, 32:2–5, 2005. doi: 10.1029/2005GL024233.

Yochanan Kushnir, Adam A Scaife, Raymond Arritt, Gianpaolo Balsamo, George Boer, Francisco Doblas-reyes, Ed Hawkins, Masahide Kimoto, and Rupa Kumar Kolli. climate. *Nature Climate Change*, 9, 2019. doi: 10.1038/s41558-018-0359-7.

M. Latif, E. Roeckner, M. Botzet, M. Esch, H. Haak, S. Hagemann, J. Jungclaus, S. Legutke, S. Marsland, U. Mikolajewicz, and J. Mitchell. Reconstructing , Monitoring , and Predicting Multidecadal-Scale Changes in the North Atlantic Thermohaline Circulation with Sea Surface Temperature. *Journal of Climate*, 17:1605–1614, 2004.

Katja Lohmann, Helge Drange, and Mats Bentsen. Response of the North Atlantic subpolar gyre to persistent North Atlantic oscillation like forcing. *Climate Dynamics*, 32:273–285, 2008. doi: 10.1007/s00382-008-0467-6.

Katja Lohmann, Helge Drange, and Mats Bentsen. A possible mechanism for the strong weakening of the North Atlantic subpolar gyre in the mid-1990s. *Geophysical Research Letters*, 36, 2009. doi: 10.1029/2009GL039166.

Michael E. Mann, Byron A. Steinman, and Sonya K. Miller. Geophysical Research Letters. *Geophysical Research Letters*, pages 3211–3219, 2014. doi: 10.1002/2014GL059233.Received.

Michael E Mann, Byron A Steinman, and Sonya K Miller. Absence of internal multidecadal and interdecadal oscillations in climate model simulations. *Nature Communications*, pages 1–9, 2020. ISSN 2041-1723. doi: 10.1038/s41467-019-13823-w. URL `http://dx.doi.org/10.1038/s41467-019-13823-w`.

John Marshall, Helen Johnson, and Jason Goodman. A Study of the Interaction of the North Atlantic Oscillation with Ocean Circulation. *Journal of Climate*, 14:1399–1421, 2001.

Odd Helge Otterå, Mats Bentsen, Helge Drange, and Lingling Suo. External forcing as a metronome for Atlantic multidecadal variability. *Nature Geoscience*, 3(10):1–6, 2010. ISSN 1752-0894. doi: 10.1038/ngeo955. URL `http://dx.doi.org/10.1038/ngeo955`.

Yannick Peings and Gudrun Magnusdottir. Forcing of the wintertime atmospheric circulation by the multidecadal fluctuations of the North Atlantic ocean. *Environmental Research Letters*, 9, 2014. doi: 10.1088/1748-9326/9/3/034018.

Jon Robson, Rowan Sutton, Katja Lohmann, Dough Smith, and Matthew Palmer. Causes of the Rapid Warming of the North Atlantic Ocean in the Mid-1990s. *Journal of Climate*, 25:4116–4134, 2012. doi: 10.1175/JCLI-D-11-00443.1.

Jon Robson, Irene Polo, Dan L R Hodson, David P Stevens, and Len C Shaffrey. Decadal prediction of the North Atlantic subpolar gyre in the HiGEM high - resolution climate model. *Climate Dynamics*, 50:921–937, 2018. doi: 10.1007/s00382-017-3649-2.

Torben Schmith, Shuting Yang, Emily Gleeson, and Tido Semmler. How Much Have Variations in the Meridional Overturning Circulation Contributed to Sea Surface Temperature Trends since 1850 ? A Study with the EC-Earth Global Climate Model. *Journal of Climate*, 27:6343–6357, 2014. doi: 10.1175/JCLI-D-13-00651.1.

D M Smith, R Eade, A A Scaife, L Caron, G Danabasoglu, T M Delsole, and T Delworth. Robust skill of decadal climate predictions. *npj Climate and Atmospheric Science*, 13, 2019. doi: 10.1038/s41612-019-0071-y.

Rowan T Sutton and Daniel L R Hodson. Atlantic Ocean Forcing of North American and European Summer Climate. *Science*, 309, 2005.

A. Timmermann, M. Latif, R. Voss, and A. Grötzner. Northern Hemispheric Interdecadal Variability : A Coupled Air-Sea Mode Northern Hemispheric Interdecadal Variability : A Coupled Air – Sea Mode. *Journal of Climate*, 11, 1998. doi: 10.1175/1520-0442-11.8.1906.

Martin Visbeck, Eric P Chassignet, Ruth Curry, Tom Delworth, Bob Dickson, and Gerd Krahmann. 6 . The Ocean ' s Response to North Atlantic Oscillation Variability. *Geophysical Monograph Series*, 2003. doi: 10.1029/134GM06.

Martin H Visbeck, James W Hurrell, Lorenzo Polvani, and Heidi M Cullen. From the Academy The North Atlantic Oscillation : Past , present , and future. *Proceedings of the National Academy of Sciences*, 98, 2001.

Chunzai Wang, Liping Zhang, Sang-ki Lee, Lixin Wu, and Carlos R Mechoso. A global perspective on CMIP5 climate model biases. *Nature Climate Change*, 4, 2014. doi: 10.1038/NCLIMATE2118.

Yiguo Wang, François Counillon, Ingo Bethke, Noel Keenlyside, and Marc Bocquet. Optimising assimilation of hydrographic profiles into isopycnal ocean models with ensemble data assimilation. *Ocean Modelling*, 114:33–44, 2017. ISSN 1463-5003. doi: 10.1016/j.ocemod.2017.04.007. URL `http://dx.doi.org/10.1016/j.ocemod.2017.04.007`.

Masahiro Watanabe and Hiroaki Tatebe. Reconciling roles of sulphate aerosol forcing and internal variability in Atlantic multidecadal climate changes. *Climate Dynamics*, 53(7):4651–4665, 2019. ISSN 1432-0894. doi: 10.1007/s00382-019-04811-3. URL `https://doi.org/10.1007/s00382-019-04811-3`.

Ayako Yamamoto, Hiroaki Tatebe, and Masami Nonaka. On the Emergence of the Atlantic Multidecadal SST Signal : A Key Role of the Mixed Layer Depth Variability Driven by North Atlantic Oscillation. *Journal of Climate*, 33:3511–3531, 2020. doi: 10.1175/JCLI-D-19-0283.1.

Xiaoqin Yan, Rong Zhang, and Thomas R Knutson. The role of Atlantic overturning circulation in the recent decline of Atlantic major hurricane frequency. *Nature Communications*, 8:1–7, 2017. ISSN 2041-1723. doi: 10.1038/s41467-017-01377-8. URL `http://dx.doi.org/10.1038/s41467-017-01377-8`.

Xiaoqin Yan, Rong Zhang, and Thomas R. Knutson. Underestimated AMOC Variability and Implications for AMV and Predictability in CMIP Models. *Geophysical Research Letters*, pages 4319–4328, 2018. doi: 10.1029/2018GL077378.

S G Yeager and J I Robson. Recent Progress in Understanding and Predicting Atlantic Decadal Climate Variability. *Current Climate Change Reports*, 3:112–127, 2017. doi: 10.1007/s40641-017-0064-z.

S. G Yeager, G. Danabasoglu, N. A. Rosenbloom, W. Strand, S. C. Bates, G. A. Meehl, A. Karspeck, K. Lindsay, M. C. Long, H. Teng, and N. S. Lovenduski. A Large Ensemble of Initialized Decadal Prediction. *Bulletin of the American Meteorological Society*, 99:1867–1886, 2018. doi: 10.1175/BAMS-D-17-0098.1.

Stephen Yeager, Alicia Karspeck, Gokhan Danabasoglu, Joe Tribbia, and Haiyan Teng. A decadal prediction case study: Late twentieth-century north Atlantic Ocean heat content. *Journal of Climate*, 25(15):5173–5189, 2012. ISSN 08948755. doi: 10.1175/JCLI-D-11-00595.1. URL `http://atoc.colorado.edu/ milliff/ATOC-6020-814/Lectures/Yeager_etal_JClim2012.pdf`.

Davide Zanchettin, Oliver Bothe, Wolfgang Müller, Jürgen Bader, and Johann H Jungclaus. Different flavors of the Atlantic Multidecadal Variability. *Climate Dynamics*, 42, 2014. doi: 10.1007/s00382-013-1669-0.

Liping Zhang and Chunzai Wang. Multidecadal North Atlantic sea surface temperature and Atlantic meridional overturning circulation variability in CMIP5 historical simulations. *Journal of Geophysical Research*, 118:5772–5791, 2013. doi: 10.1002/jgrc.20390.

Rong Zhang. Mechanisms for low-frequency variability of summer Arctic sea ice extent. *Proceedings of the National Academy of Sciences*, 112, 2015. doi: 10.1073/pnas.1422296112.

Rong Zhang and Thomas L Delworth. Impact of Atlantic multidecadal oscillations on India / Sahel rainfall and Atlantic hurricanes. *Geophysical Research Letters*, 33, 2006. doi: 10.1029/2006GL026267.

Rong Zhang, Thomas L Delworth, and Isaac M Held. Can the Atlantic Ocean drive the observed multidecadal variability in Northern Hemisphere mean temperature ? *Geophysical Research Letters*, 34, 2007. doi: 10.1029/2006GL028683.

Rong Zhang, Rowan Sutton, Gokhan Danabasoglu, Thomas L Delworth, Who M Kim, Jon Robson, and Stephen G Yeager. Comment on "The Atlantic Multidecadal Oscillation without a role for ocean circulation". *Science*, 352(6293):1527, 2016. ISSN 0036-8075. doi: 10.1126/science.aaf1660. URL `http://science.sciencemag.org/content/352/6293/1527.1`.

Rong Zhang, Rowan Sutton, Gokhan Danabasoglu, and Young Oh Kwon. A Review of the Role of the Atlantic Meridional Overturning Circulation in Atlantic Multidecadal Variability and Associated Climate Impacts. *Reviews of Geophysics*, pages 1–60, 2019. doi: 10.1029/2019RG000644.

References, observational data

Boyin Huang, Peter W. Thorne, Viva F. Banzon, Tim Boyer, Gennady Chepurin, Jay H. Lawrimore, Matthew J. Menne, Thomas M. Smith, Russell S. Vose, and Huai-Min Zhang (2017): NOAA Extended Reconstructed Sea Surface Temperature (ERSST), Version 5. [sst.mnmean.nc]. NOAA National Centers for Environmental Information. doi:10.7289/V5T72FNM [18.11.2019]

Yu, Lisan and Weller, Robert A.: WHOI OAFlux project. Last modified 03.11.2011. Retrieved from $ftp://ftp.whoi.edu/pub/science/oaflux/data_v3/monthly/netheat\_1983-2009/$.

Hurrell, James and National Center for Atmospheric Research Staff (Eds). Last modified 24.04.2020. "The Climate Data Guide: Hurrell North Atlantic Oscillation (NAO) Index (station-based)." Retrieved from $https://climatedataguide.ucar.edu/climate-data/hurrell-north-atlantic-oscillation-nao-index-station-based$.

Smeed D.; Moat B; Rayner D.; Johns W.E.; Baringer M.O.; Volkov D.; Frajka-Williams E. (2019). Atlantic meridional overturning circulation observed by the RAPID-MOCHA-WBTS (RAPID-Meridional Overturning Circulation and Heatflux Array-Western Boundary Time Series) array at 26N from 2004 to 2018. British Oceanographic Data Centre - Natural Environment Research Council, UK. doi: 10.5285/8cd7e7bb-9a20-05d8-e053-6c86abc012c2.